

Coupling Polyatomic Molecules to Lossy Nanocavities: Lindblad versus Schrödinger description

Csaba Fábri,^{1,2, a)} Attila G. Császár,^{1,3} Gábor J. Halász,⁴ Lorenz S. Cederbaum,⁵ and Ágnes Vibók^{2,6, b)}

¹⁾*HUN-REN-ELTE Complex Chemical Systems Research Group, P.O. Box 32, H-1518 Budapest 112, Hungary*

²⁾*Department of Theoretical Physics, University of Debrecen, P.O. Box 400, H-4002 Debrecen, Hungary*

³⁾*Laboratory of Molecular Structure and Dynamics, Institute of Chemistry, ELTE Eötvös Loránd University, H-1117 Budapest, Pázmány Péter sétány 1/A, Hungary*

⁴⁾*Department of Information Technology, University of Debrecen, P.O. Box 400, H-4002 Debrecen, Hungary*

⁵⁾*Theoretische Chemie, Physikalisch-Chemisches Institut, Universität Heidelberg, D-69120 Heidelberg, Germany*

⁶⁾*ELI-ALPS, ELI-HU Non-Profit Ltd, H-6720 Szeged, Dugonics tér 13, Hungary*

(Dated: 22 May 2024)

The use of cavities to impact molecular structure and dynamics has become popular. As cavities, in particular plasmonic nanocavities, are lossy and the lifetime of their modes can be very short, their lossy nature must be incorporated into the calculations. The Lindblad master equation is commonly considered as an appropriate tool to describe this lossy nature. This approach requires the dynamics of the density operator and is thus substantially more costly than approaches employing the Schrödinger equation for the quantum wave function when several or many nuclear degrees of freedom are involved. In this work we compare numerically the Lindblad and Schrödinger descriptions discussed in the literature for a molecular example where the cavity is pumped by a laser. The laser and cavity properties are varied over a range of parameters. It is found that the Schrödinger description adequately describes the dynamics of the polaritons and emission signal as long as the laser intensity is moderate and the pump time is not much longer than the lifetime of the cavity mode. Otherwise, it is demonstrated that the Schrödinger description gradually fails. We also show that the failure of the Schrödinger description can often be remedied by renormalizing the wave function at every step of the time propagation. The results are discussed and analyzed.

^{a)}Electronic mail: ficsaba@staff.elte.hu

^{b)}Electronic mail: vibok@phys.unideb.hu

I. INTRODUCTION

Polyatomic quantum emitters offer a high degree of complexity as electron-photon interactions are strongly influenced by the coupling of the electrons to nuclear vibrational and rotational motions. The confined photonic mode of the cavity can resonantly couple to the transition dipole of the molecule, giving rise to mixed polaritonic states carrying both photonic and excitonic features.¹ A vast number of experimental^{2–11} and theoretical^{12–52} works have demonstrated that hybrid light-matter polaritons can dramatically modify and even control static and dynamic features of matter. Interesting applications have reported the enhancement or suppression of photochemical processes, reaction rates^{24,27,53–56} and isomerization,^{57,58} the modification of charge⁵⁹ or electron^{60–62} transfer between molecules, as well as the emergence of light-induced nonadiabatic effects,^{13,14,18,20–22,26,32,36,37,52,63–72} and so forth.

To successfully modify and control molecular properties one has to reach the strong light-matter coupling regime. This can only be achieved when the coupling strength between light and matter excitations becomes larger than the dissipation rates of the cavity mode and molecular excited states, which can be easily realized for a macroscopic number of molecules coupled to an optical or plasmonic cavity mode. As for single-molecule experiments, the situation is more complicated.⁷ In this case, strong subwavelength-size confinement is required to reach the strong-coupling limit at room temperature with typical transition dipole moment values of organic molecules, which is feasible only in plasmonic nanocavities. The latter, however, may possess a very lossy nature, because a relevant part of the energy of the nanocavity mode is stored in the kinetic energy of electrons in the metal. The lifetime of plasmonic nanocavity modes is very short, typically on the order of a few tens of femtoseconds, which must be adequately addressed in numerical simulations.

In the present work, we investigate the quantum dynamics of a single polyatomic molecule interacting with a lossy plasmonic nanocavity in the strong coupling regime. Generally, the photon loss in such a quantum system can be described by coupling the cavity-molecule system to a dissipative Markovian environment, leading to the Lindblad master equation formalism.^{30,56,70,71,73,74} In this situation, the temporal evolution of the system can be obtained by propagating the density matrix in time, according to the appropriate Lindblad master equation. However, cavity loss can be incorporated in the time-dependent

Schrödinger equation (TDSE) framework as well.^{75,76} This is an alternative and frequently used description of how a photon can escape from a cavity, but the adequacy of this description needs to be explored. If quantum dynamics is restricted to a certain excitation manifold (such as the singly-excited subspace, that is, ground-state molecule with one photon and excited-state molecule with zero photons), dissipative effects can be described by a non-Hermitian formalism in which the Hamiltonian of the system is augmented with an imaginary term. The effective non-Hermitian Hamiltonian obtained in this manner implicitly includes the cavity leakage which is then accounted for by a loss of norm of the nuclear wave packet during time propagation using the TDSE.

In this paper, the performance of the non-Hermitian TDSE method is compared to that of the Lindblad-master-equation approach. To carry out a thorough comparison of the two methods, different cavity and laser pumping parameters are applied. As a showcase system, the four-atomic formaldehyde (H_2CO) molecule is applied. It is demonstrated that if the lower (1LP) and upper (1UP) polaritonic states in the singly-excited subspace are driven with a pump pulse, the TDSE with a non-Hermitian Hamiltonian works very well in many cases as long as excited-state populations and cavity emission are of primary interest. Therefore, it is worth examining the range of validity of the Schrödinger-based description, also due to its more favorable computational cost. The Lindblad-master-equation approach is known to be computationally more demanding than the TDSE, as the state of the system is represented by a density matrix (instead of a state vector) and matrix-matrix multiplications have to be performed during the time evolution. Another important advantage of the non-Hermitian TDSE is that it enables the inclusion of molecular rotational degrees of freedom in the quantum-dynamical description^{77,78} due to its lower computational cost compared to the Lindblad-based description. Thus, the non-Hermitian TDSE offers a correct treatment of light-induced nonadiabatic properties of small diatomic molecules in a lossy nanocavity.

However, in several situations, results of the Lindblad and non-Hermitian TDSE approaches differ significantly. For example, the ground-state Schrödinger and Lindblad populations are always different. It is also shown that the Schrödinger and Lindblad results can deviate substantially if the lifetime of the cavity mode is short relative to the length of the pump pulse. Moreover, excitation above the singly-excited subspace can also lead to visible differences between the two approaches. We will also demonstrate that these discrepancies between the Lindblad and non-Hermitian TDSE approaches can often be remedied by set-

ting the norm of the wave function to one at each step of the time propagation in case of the non-Hermitian TDSE (renormalized TDSE method).

A similar comparison of the Lindblad and non-Hermitian TDSE methods has recently been presented in Ref. 79 where the non-Hermitian TDSE approach has been found to often provide adequate results for quantum dots coupled to a plasmonic mode. Another relevant work is Ref. 80 where a non-Hermitian Schrödinger equation was employed to develop a cavity quantum electrodynamics model for dissipative photonic modes using the configuration interaction singles method. Finally, it is worth noting that a compromise between the Lindblad and non-Hermitian TDSE approaches could be the stochastic Schrödinger method based on the Monte Carlo wave packet formalism.^{81–83}

The structure of the paper is as follows. Section II provides the (i) theoretical description of the lossy cavity-molecule system, (ii) Lindblad-master-equation approach, (iii) non-Hermitian TDSE approach, and (iv) a brief summary of the computational model used for the H₂CO molecule. Section III presents and discusses the results of the quantum-dynamical computations, while conclusions and outlook are provided in Section IV. In addition, results with the renormalized TDSE method, density matrix purities and results with a special initial state are given in Appendix A and B.

II. THEORY AND COMPUTATIONAL PROTOCOL

A single molecule interacting with a cavity mode can be described by the Hamiltonian⁸⁴

$$\hat{H}_{\text{cm}} = \hat{H}_0 + \hbar\omega_c \hat{a}^\dagger \hat{a} - g \hat{\mu} \vec{e} (\hat{a}^\dagger + \hat{a}) + \frac{g^2}{\hbar\omega_c} (\hat{\mu} \vec{e})^2 \quad (1)$$

where \hat{H}_0 is the Hamiltonian of the isolated (field-free) molecule, ω_c denotes the cavity-mode angular frequency, \hat{a}^\dagger and \hat{a} are creation and annihilation operators of the cavity mode, $\hat{\mu}$ is the electric dipole moment operator of the molecule and \vec{e} corresponds to the cavity field polarization vector. The coupling between the molecule and the cavity mode is described by the coupling strength parameter $g = \sqrt{\frac{\hbar\omega_c}{2\epsilon_0 V}}$ where ϵ_0 and V are the permittivity and quantization volume of the cavity, respectively. The last term of \hat{H}_{cm} is the so-called dipole self-energy.^{29,42,52,85–88} In this work, we consider a single molecule coupled to a plasmonic cavity mode and omit the dipole self-energy (DSE) term (see Refs. 42, 89, and 90 for further explanation).

In one takes into account two molecular electronic states (X and A), \hat{H}_{cm} can be recast as

$$\hat{H}_{\text{cm}} = \begin{bmatrix} \hat{T} + V_X & 0 & W_X^{(1)} & W_{XA}^{(1)} & 0 & 0 & \dots \\ 0 & \hat{T} + V_A & W_{XA}^{(1)} & W_A^{(1)} & 0 & 0 & \dots \\ W_X^{(1)} & W_{XA}^{(1)} & \hat{T} + V_X + \hbar\omega_c & 0 & W_X^{(2)} & W_{XA}^{(2)} & \dots \\ W_{XA}^{(1)} & W_A^{(1)} & 0 & \hat{T} + V_A + \hbar\omega_c & W_{XA}^{(2)} & W_A^{(2)} & \dots \\ 0 & 0 & W_X^{(2)} & W_{XA}^{(2)} & \hat{T} + V_X + 2\hbar\omega_c & 0 & \dots \\ 0 & 0 & W_{XA}^{(2)} & W_A^{(2)} & 0 & \hat{T} + V_A + 2\hbar\omega_c & \dots \\ \vdots & \vdots & \vdots & \vdots & \vdots & \vdots & \ddots \end{bmatrix} \quad (2)$$

where \hat{T} is the nuclear (rotational-vibrational) kinetic energy operator, while V_X and V_A are the electronic ground-state and excited-state potential energy surfaces (PESs) of the molecule. The cavity-molecule coupling is described by the operators $W_\alpha^{(n)} = -g\sqrt{n}\mu_\alpha$ ($\alpha = X, A$) and $W_{XA}^{(n)} = -g\sqrt{n}\mu_{XA}$ where Fock states of the cavity mode are labeled by the quantum number $n = 0, 1, 2, \dots$. Projections of the permanent (PDM) and transition (TDM) dipole moments along \vec{e} are denoted by μ_α ($\alpha = X, A$) and μ_{XA} , respectively. The Hamiltonian \hat{H}_{cm} of Eq. (1) corresponds to the so-called diabatic representation. Polaritonic (adiabatic) PESs can be obtained as eigenvalues of the potential energy part of \hat{H}_{cm} at each nuclear configuration. Under strong coupling, the ground (lowest) polaritonic state essentially equals $|X0\rangle$ (electronic ground state with zero photons), while the lower (1LP) and upper (1UP) polaritonic states can be well approximated as the linear combinations of $|X1\rangle$ and $|A0\rangle$ (singly-excited subspace).

\hat{H}_{cm} of Eq. (1) clearly assumes an infinite lifetime for field excitations. However, the highly lossy nature of plasmonic nanocavities requires that finite photon lifetimes are taken into account. As already outlined in Section I, this can be achieved by the Lindblad master equation⁷³

$$\frac{\partial \hat{\rho}}{\partial t} = -\frac{i}{\hbar}[\hat{H}, \hat{\rho}] + \gamma_c \hat{a} \hat{\rho} \hat{a}^\dagger - \frac{\gamma_c}{2}(\hat{\rho} \hat{N} + \hat{N} \hat{\rho}) \quad (3)$$

where $\hat{\rho}$ denotes the density operator and $\hat{N} = \hat{a}^\dagger \hat{a}$ is the photon number operator associated with the cavity mode. Moreover, γ_c specifies the cavity decay rate which is equivalent to a lifetime of $\tau = 1/\gamma_c$. In Eq. (3), \hat{H}_{cm} is supplemented with a term which describes the interaction of the cavity mode with a pump laser pulse, that is,

$$\hat{H} = \hat{H}_{\text{cm}} - \mu_c E(t)(\hat{a}^\dagger + \hat{a}) \quad (4)$$

where $\mu_c = 1.0$ au (effective dipole moment of the cavity mode) and the pump pulse is specified by $E(t) = E_0 \sin^2(\pi t/T) \cos(\omega t)$ for $0 \leq t \leq T$ and $E(t) \equiv 0$ otherwise. E_0 , T and ω denote the amplitude, length and carrier angular frequency of the pump pulse, respectively. E_0 can be converted into laser intensity by the formula $I = c\epsilon_0 E_0^2/2$ (c is the speed of light in vacuum and ϵ_0 is the vacuum permittivity). Following Ref. 30, we take the radiative emission rate E_R to be proportional to the expectation value of \hat{N} , which yields $E_R \sim \text{Tr}(\hat{\rho}\hat{N}) = N(t)$. As the lifetime of excited electronic states typically exceeds the cavity lifetimes applied in the current work, we assume an infinite lifetime for the excited electronic state.

As explained in Ref. 91, dissipation during the time evolution of an open quantum system can be described by the non-Hermitian time-dependent Schrödinger equation (TDSE). In our case, the TDSE takes the form

$$i\hbar \frac{\partial |\Psi\rangle}{\partial t} = \left(\hat{H} - i\frac{\gamma_c}{2} \hat{N} \right) |\Psi\rangle \quad (5)$$

where the Hamiltonian $\hat{H} - i\frac{\gamma_c}{2} \hat{N}$ is clearly non-Hermitian. It is also shown in Ref. 91 that the Lindblad master equation without the term $\gamma_c \hat{a} \hat{\rho} \hat{a}^\dagger$ is equivalent to the TDSE of Eq. (5). The term $\gamma_c \hat{a} \hat{\rho} \hat{a}^\dagger$ induces incoherent transitions $|\alpha(n+1)\rangle \rightarrow |\alpha n\rangle$ (α labels molecular electronic states X and A). This way, population losses in the states $|\alpha n\rangle$ with $n > 0$ are compensated and the space integral of the density is conserved by the Lindblad master equation. Obviously, if one employs the non-Hermitian TDSE, this is not the case and the norm of the wave function decreases over time due to the term $-i\frac{\gamma_c}{2} \hat{N}$ in Eq. (5). As we will see, one way of improving the non-Hermitian TDSE method is to set the norm of the wave function to one at each time step during the time propagation, which is also applied by the stochastic Schrödinger method.⁸¹ The time evolution can be expressed in terms of the state vector $|\Psi\rangle$ instead of $\hat{\rho}$ if the TDSE is used, which significantly reduces the cost of time propagation in particular if several or many nuclear degrees of freedom are involved. Consequently, knowing where the Schrödinger approach is a good approximation is extremely relevant.

Next, the computational model used for the formaldehyde (H_2CO) molecule is described briefly. We consider the two singlet electronic states S_0 (\tilde{X}^1A_1) and S_1 (\tilde{A}^1A_2) of H_2CO and treat the ν_2 (C=O stretch) and ν_4 (out-of-plane) vibrational modes (2D(ν_2, ν_4) vibrational model) in all computations. We stress that the 2D(ν_2, ν_4) model has been shown to provide

a physically correct description of the X→A electronic spectrum of H₂CO.^{26,36} In addition, the three rotational degrees of freedom are omitted and the molecular orientation is kept fixed with respect to the polarization vector (\vec{e}) of the cavity field. In the 2D(ν_2, ν_4) model, the PDMs are orthogonal to the TDM. Therefore, as \vec{e} is chosen to be parallel with the TDM in the current work, the PDMs are orthogonal to \vec{e} and the terms $W_\alpha^{(n)}$ vanish in Eq. (2). We refer to Refs. 26, 37, 70, 71, and 92 for further details of the 2D(ν_2, ν_4) vibrational model.

In case of the Lindblad master equation, the state of the coupled cavity-molecule system is given by the density operator $\hat{\rho}$. In order to facilitate numerical computations, $\hat{\rho}$ is represented in the basis $|\alpha in\rangle$ where $\alpha = X, A$ labels molecular electronic states, i denotes two-dimensional direct-product discrete variable representation (DVR)^{93,94} basis functions and $n = 0, 1, 2, 3$. In the current work, an equidistant Fourier DVR⁹⁵ has been employed for both the ν_2 and ν_4 vibrational modes. For the TDSE, one can again utilize the basis $|\alpha in\rangle$ to represent $|\Psi\rangle$. The Lindblad master equation and the TDSE are integrated with the explicit third-order Adams–Bashforth method.⁹⁶

In the next section, results (populations of polaritonic states and photon emission signal) with several different cavity and laser parameters will be presented. In all cases, the system is prepared in a pure initial state with $\hat{\rho}(t=0) = |\Psi_0\rangle\langle\Psi_0|$ (Lindblad) or $|\Psi(t=0)\rangle = |\Psi_0\rangle$ (TDSE) where $|\Psi_0\rangle$ is the ground state of the coupled cavity-molecule system. Then, the system is excited by a pump laser pulse which in most cases is chosen such that it transfers population primarily to the singly-excited subspace, either to the 1LP or to the 1UP states. One-dimensional diabatic PES cuts along the vibrational mode ν_2 and two-dimensional 1LP and 1UP PESs are depicted in Fig. 1 for the cavity parameters $\omega_c = 29957.2 \text{ cm}^{-1}$ and $g = 0.02 \text{ au}$. Occasionally, higher-lying polaritonic states will be populated as well, which will shed further light on the difference between the Lindblad and TDSE-based descriptions.

III. RESULTS AND DISCUSSION

Having described the theory, the computational protocol and the molecular system under investigation, we will now examine the populations of polaritonic states as well as the ultrafast radiative emission signal of the cavity. We will mainly focus on the 1LP and 1UP polaritonic states of the singly-excited subspace. We will discuss in detail how the different

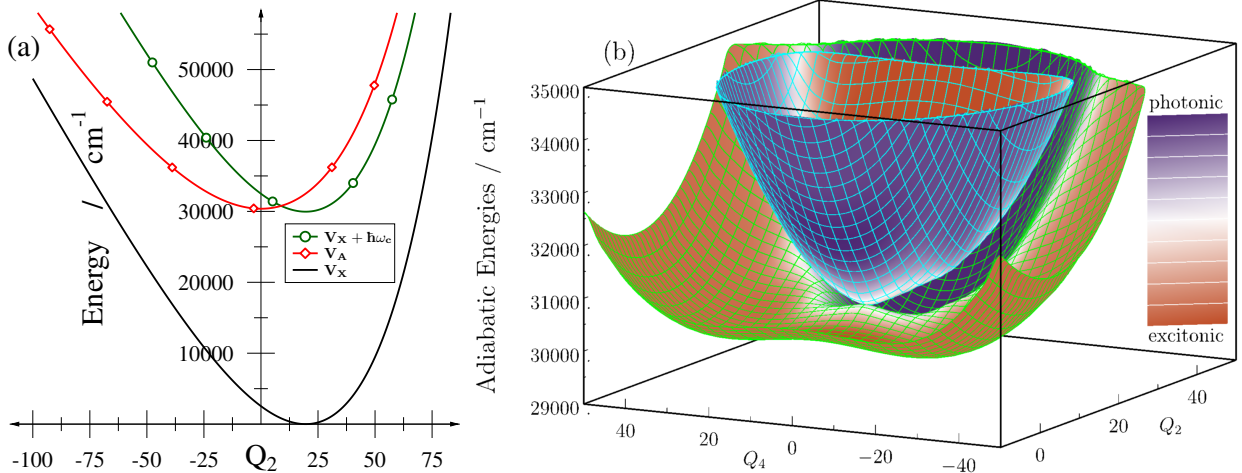


FIG. 1. (a) Diabatic potentials (V_X , V_A and $V_X + \hbar\omega_c$) as a function of the C=O stretch normal coordinate (Q_2) (the out-of-plane normal coordinate is fixed at $Q_4 = 0$). The cavity wavenumber equals $\omega_c = 29957.2 \text{ cm}^{-1}$. (b) Two-dimensional lower (1LP) and upper (1UP) polaritonic potential energy surfaces (singly-excited subspace). The cavity wavenumber and coupling strength are set to $\omega_c = 29957.2 \text{ cm}^{-1}$ and $g = 0.02 \text{ au}$, respectively. The character of the polaritonic surfaces is indicated by a purple-orange colormap (purple: photonic (ground-state molecule with one photon), orange: excitonic (excited-state molecule with zero photons)).

pump laser parameters (frequency, intensity, and pulse length) as well as the frequency, coupling strength, and decay rate of the cavity mode influence the physical quantities of interest.

A. Population transfer to the lower polariton (1LP state)

In this section all numerical results (from Fig. 2 to Fig. 5) have been obtained with $\omega = 30000 \text{ cm}^{-1}$ (carrier wavenumber of the pump laser pulse) and $\omega_c = 29957.2 \text{ cm}^{-1}$ (cavity wavenumber), while the remaining laser and cavity parameters vary from figure to figure. We note that the current ω and ω_c values correspond to case 1 of Ref. 71 where oscillations in the emission signal were attributed to wave packet motion between the photonic (ground-state molecule with one photon) and excitonic (excited-state molecule with zero photons) parts of the 1LP PES.

As for the laser parameters in Fig. 2, we have applied the values $T = 15 \text{ fs}$ (pulse length) and $I = 5 \cdot 10^{11} \text{ W/cm}^2$ (intensity). Regarding the cavity coupling strength and

decay rate parameters, the values $g = 0.01$ au as well as $\gamma_c = 0.001$ au, $\gamma_c = 0.0025$ au and $\gamma_c = 0.005$ au are used, respectively. The latter values are equivalent to lifetimes of $\tau = 1/\gamma_c = 24.2$ fs ($\gamma_c = 0.001$ au), $\tau = 9.7$ fs ($\gamma_c = 0.0025$ au) and $\tau = 4.8$ fs ($\gamma_c = 0.005$ au). In this case, the laser transfers population to the photonic part of the 1LP state with high selectivity and the ensuing quantum dynamics takes place almost entirely on the 1LP PES. This is confirmed by Fig. 2 which shows that polaritonic states above the 1LP state are hardly populated. In Fig. 2 the labels 2LP and 2UP denote polaritonic states that can be characterized as superpositions of the diabatic states $|X2\rangle$ and $|A1\rangle$ to a good approximation. The amount of population transferred to the 1LP state depends on the lifetime of the cavity photon and also on the method (Lindblad or TDSE) used. In case of the Lindblad approach, due to the incoherent transition $|X1\rangle \rightarrow |X0\rangle$ induced by the term $\gamma_c \hat{a} \hat{\rho} \hat{a}^\dagger$, part of the population is transferred back to the ground polaritonic state from 1LP already during the pumping process. This is not possible with the non-Hermitian TDSE, as the 1LP population absorbed by the imaginary part of the non-Hermitian Hamiltonian is not restored to the ground polaritonic state. Not surprisingly, higher values of γ_c lead to faster relaxation of the excited polaritonic populations and the emission signal. Larger values of γ_c are generally expected to result in larger discrepancies between the Lindblad and TDSE-based descriptions. This tendency is a direct consequence that the incoherent decay term is missing in the non-Hermitian TDSE scheme. At the same time, however, the 1LP populations and corresponding emissions agree well for the parameter ranges investigated in Fig. 2.

Fig. 3 presents results obtained with parameters different from the ones used in Fig. 2. Here we have employed the highest cavity decay rate of $\gamma_c = 0.005$ au, $g = 0.01$ au, laser intensities of $I = 5 \cdot 10^{11}$ W/cm² and $I = 10^{12}$ W/cm² and doubled the pulse duration to $T = 30$ fs from $T = 15$ fs. The results obtained differ significantly from those displayed in Fig. 2. As the laser pulse gets longer and its intensity gets higher, the non-Hermitian TDSE method breaks down spectacularly even for the populations of excited polaritonic states and for the emission signal. The reason for these observations is that the non-Hermitian TDSE does not return population to the ground polaritonic state by the incoherent decay term. As already stated, this is not the case for the Lindblad master equation. If the length of the pulse is sufficiently large compared to the cavity lifetime, the incoherent decay term starts to repopulate the ground polaritonic state before the laser pulse ends. This

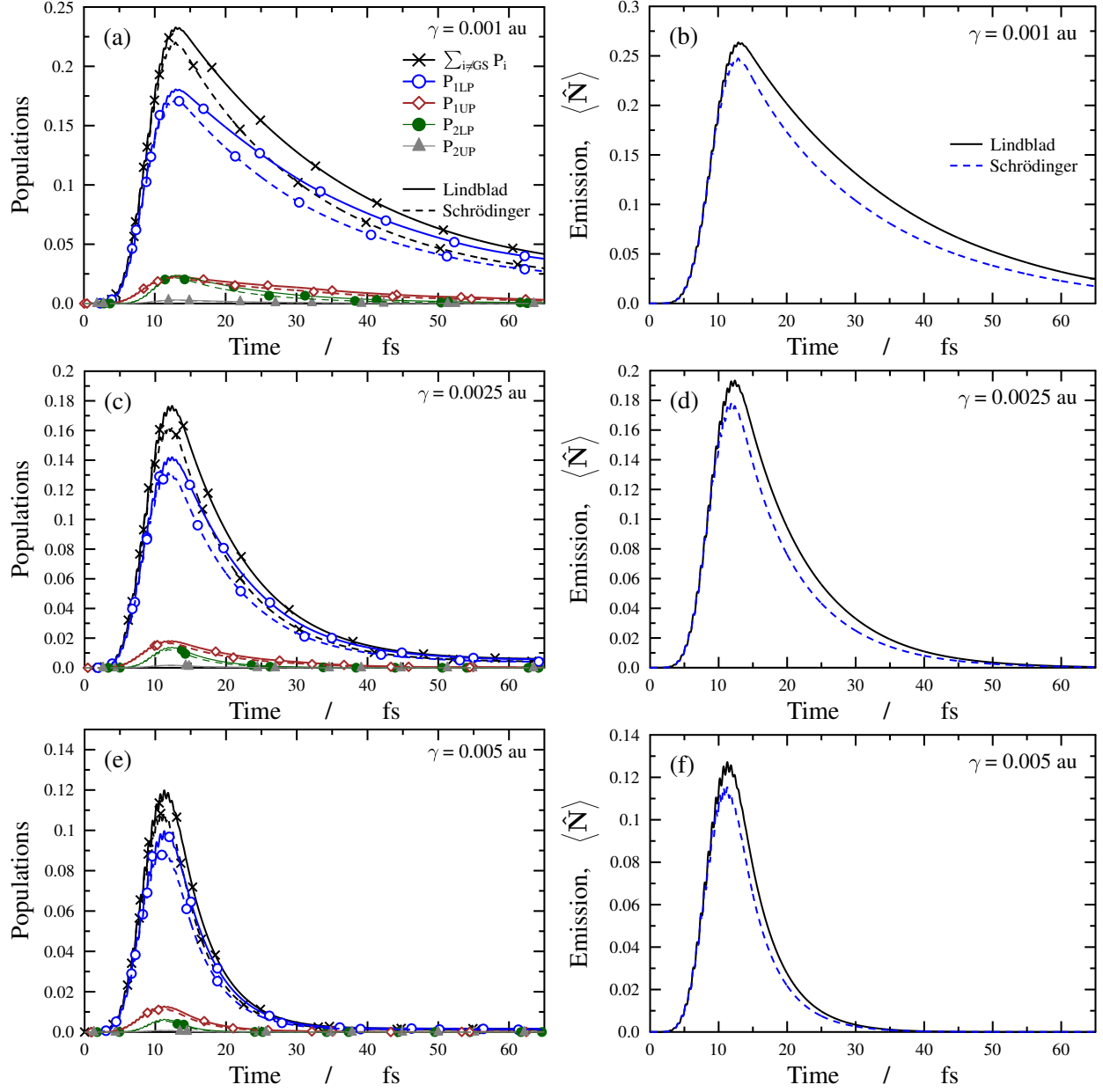


FIG. 2. Populations of polaritonic states and emission curves (the emission is proportional to the expectation value of the photon number operator \hat{N}) for cavity decay rates $\gamma_c = 0.001$ au (equivalent to a lifetime of $\tau = 24.2$ fs, panels a and b), $\gamma_c = 0.0025$ au ($\tau = 9.7$ fs, panels c and d) and $\gamma_c = 0.005$ au ($\tau = 4.8$ fs, panels e and f). The cavity wavenumber and coupling strength equal $\omega_c = 29957.2$ cm^{-1} and $g = 0.01$ au, respectively. Parameters of the pump laser pulse are chosen as $\omega = 30000$ cm^{-1} , $T = 15$ fs and $I = 5 \cdot 10^{11}$ W/cm^2 . The Lindblad results (solid lines) agree well with their Schrödinger (TDSE) counterparts (dashed lines) in all cases presented.

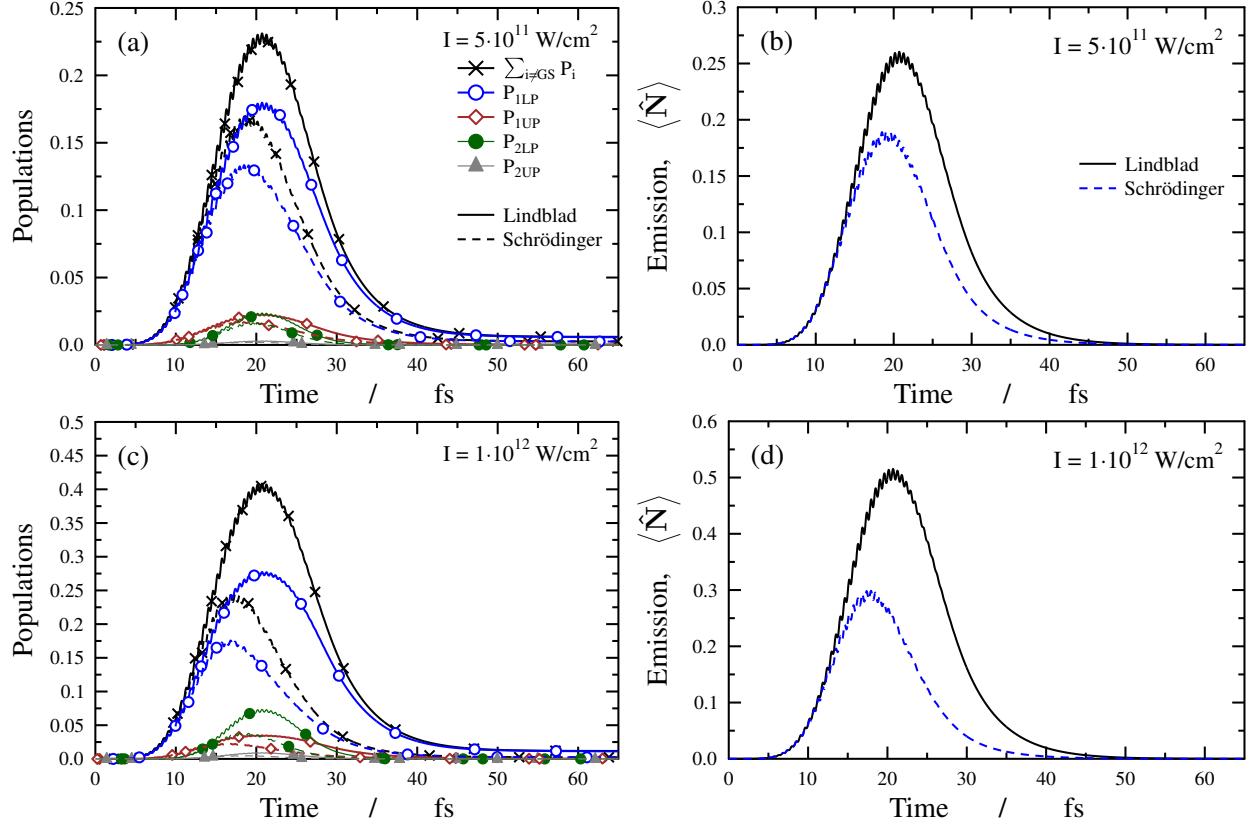


FIG. 3. Populations of polaritonic states and emission curves (the emission is proportional to the expectation value of the photon number operator \hat{N}) for laser intensities $I = 5 \cdot 10^{11} \text{ W/cm}^2$ (panels a and b) and $I = 10^{12} \text{ W/cm}^2$ (panels c and d). The cavity wavenumber and coupling strength equal $\omega_c = 29957.2 \text{ cm}^{-1}$ and $g = 0.01 \text{ au}$, respectively, while the cavity decay rate is set to $\gamma_c = 0.005 \text{ au}$ (equivalent to a lifetime of $\tau = 4.8 \text{ fs}$). Other parameters of the pump laser pulse are chosen as $\omega = 30000 \text{ cm}^{-1}$ and $T = 30 \text{ fs}$. The Lindblad results (solid lines) show visible deviations from their Schrödinger (TDSE) counterparts (dashed lines).

way, the population returned to the ground polaritonic state can be transferred again to excited polaritonic states (dominantly to the 1LP state in this case), which results in a more efficient population transfer compared to the TDSE approach. This finding explains why the Lindblad 1LP population and emission values exceed their TDSE counterparts in Fig. 3. One can also notice that there is some population transfer above the singly-excited subspace. This is potentially interesting as the decay is faster for larger photon numbers and in the Lindblad case population in the singly-excited subspace can be replenished from higher-lying polaritonic states by the incoherent decay term.

The trends observed in Fig. 3 are even more pronounced in Fig. 4. Here the pump pulse is even longer ($T = 45$ fs) with $I = 10^{12}$ W/cm² and the coupling strength is doubled from $g = 0.01$ au to $g = 0.02$ au with $\gamma_c = 0.005$ au. We can again observe the breakdown of the non-Hermitian TDSE method and there is visible population transfer above the singly-excited subspace. Moreover, panel c of Fig. 4 shows another interesting effect, namely, for $g = 0.02$ au a certain amount of the population is trapped in the 1LP PES in the Lindblad case. Such trapping is also noticeable in panel a of Fig. 4 ($g = 0.01$ au), although to a lesser extent. The use of longer pulses and higher laser intensities facilitates the population of higher excited polaritonic states (mainly the 2LP state), from where the Lindblad scheme can transfer population back to the singly-excited subspace. In addition, the laser pulse can also transfer some population already relaxed to the ground polaritonic state back to 1LP since the pulse length T is considerably larger than the cavity lifetime τ ($T = 45$ fs $>$ $\tau = 4.8$ fs in this case). The combination of these two effects gives rise to appreciable Lindblad 1LP population at the end of the laser pulse, while in the non-Hermitian TDSE case the 1LP is essentially zero at $t = 45$ fs. The origin of the trapping mechanism is elucidated by probability density figures shown in Fig. 5. The Lindblad probability densities reveal that the pump pulse indeed transfers population to the photonic region of the 1LP PES (see panel a of Fig. 5 at $t = 30$ fs). Subsequently, the wave packet splits into two parts and moves to the excitonic region of the 1LP PES (panel b, $t = 60$ fs), which quenches photon emission and results in the trapping effect mentioned. Of course, for longer times, the wave packet will move back to the photonic region, leading to decay to the ground polaritonic state. It is conspicuous in Fig. 1 (panel b) that the 1LP PES has two symmetry-equivalent local minima which can trap the wave packet in the excitonic region for some time.

We have repeated the TDSE calculations of this section by setting norm of the wave function to one at every time step (renormalized TDSE approach). Results are presented in Appendix A (for population and emission results see Figs. 11, 13 and 15 which correspond to the parameters of Figs. 2, 3 and 4, respectively). It is clearly visible that the renormalized TDSE method greatly reduces the discrepancy between the Lindblad and TDSE results. This finding can be attributed to the renormalization of the wave function, which refills the population of the ground (lowest) polaritonic state. In addition, the purity of the density matrix, $\text{tr}(\hat{\rho}^2)$, is also given as a function of time in Appendix A (see Figs. 12, 14 and 16). In all cases considered in this section, the purity is exactly one at $t = 0$ and remains close

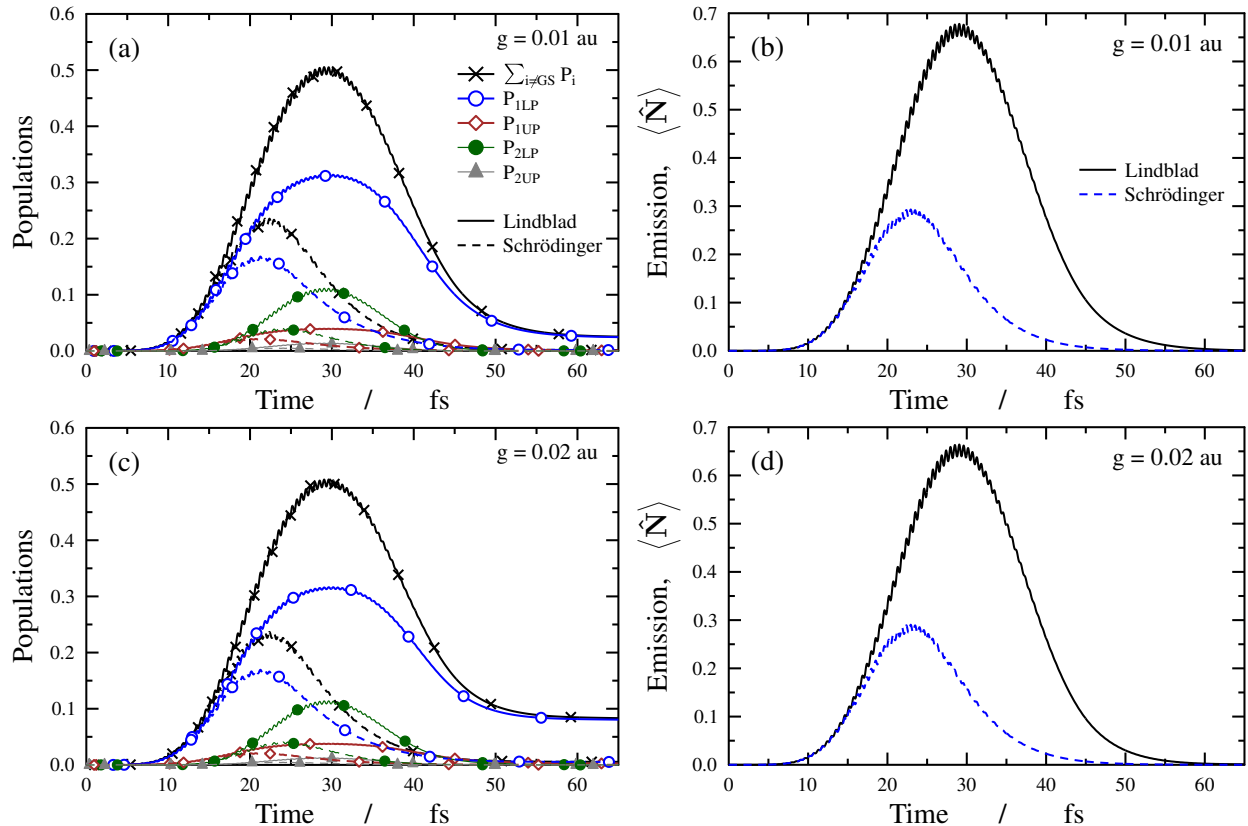


FIG. 4. Populations of polaritonic states and emission curves (the emission is proportional to the expectation value of the photon number operator \hat{N}) for coupling strength values of $g = 0.01$ au (panels a and b) and $g = 0.02$ au (panels c and d). The cavity wavenumber and decay rate equal $\omega_c = 29957.2 \text{ cm}^{-1}$ and $\gamma_c = 0.005$ au (equivalent to a lifetime of $\tau = 4.8$ fs), respectively. Parameters of the pump laser pulse are chosen as $\omega = 30000 \text{ cm}^{-1}$, $T = 45$ fs and $I = 10^{12} \text{ W/cm}^2$. The Lindblad results (solid lines) differ substantially from their Schrödinger (TDSE) counterparts (dashed lines).

to one during and after excitation.

Finally, reference results with a special initial state (molecule in the vibrational ground state of the ground (X) electronic state and 1 photon in the cavity mode) are outlined (see Appendix B). The cavity parameters are chosen as $\omega_c = 29957.2 \text{ cm}^{-1}$, $g = 0.01$ au and $\gamma_c = 0.001$ au. With this special setup, the singly-excited subspace (1LP and 1UP states) is populated at $t = 0$. Fig. 23 compares populations of polaritonic states (panel a) and emission curves (panel b) obtained with the Lindblad and non-Hermitian TDSE methods, showing good agreement. On the contrary, the Lindblad and renormalized TDSE populations and

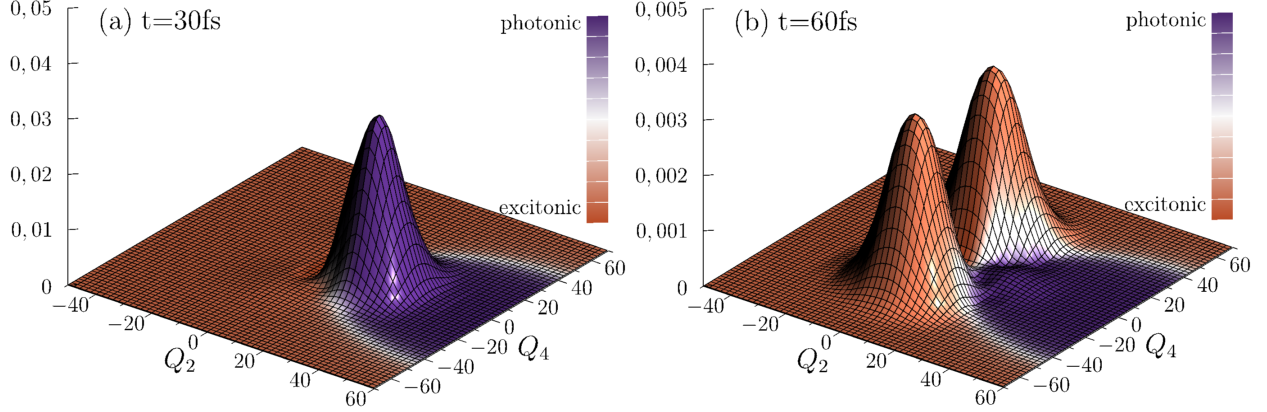


FIG. 5. Probability density figures (obtained with the Lindblad equation) for the lower polaritonic (1LP) potential energy surface at $t = 30$ fs (panel a) and $t = 60$ fs (panel b). The cavity wavenumber, coupling strength and decay rate equal $\omega_c = 29957.2$ cm^{-1} , $g = 0.02$ au and $\gamma_c = 0.005$ au, respectively. Parameters of the pump laser pulse are chosen as $\omega = 30000$ cm^{-1} , $T = 45$ fs and $I = 10^{12}$ W/cm^2 . The laser pulse mainly populates the 1LP state (and also the 2LP state to a lesser extent) in this case. At $t = 30$ fs and $t = 60$ fs the wave packet is localized in the photonic (purple) and excitonic (orange) regions of the 1LP PES, respectively.

emissions (see panels a and b of Fig. 24) show substantial deviations. The breakdown of the renormalized TDSE method can be readily rationalized by keeping in mind that the ground polaritonic state initially bears negligible population. In this case, renormalization of the wave function will keep the population trapped in the singly-excited subspace and the ground polaritonic state can not be refilled. This is to be contrasted with the previous cases where the laser pulse has transferred a certain amount of population from the ground polaritonic state to the singly-excited subspace and occasionally to higher-lying polaritonic states. Finally, Fig. 25 presents purity results (see the curve labeled as LP). As the initial state of the system is a pure state, the purity equals one at $t = 0$. Later, the system evolves into a mixed state and the purity gradually decreases to about 0.5. As relaxation continues to transfer population to the ground polaritonic state, the purity starts increasing again.

B. Population transfer to the upper polariton (1UP state)

In this case, the laser and cavity wavenumbers are set to $\omega = 36000$ cm^{-1} and $\omega_c = 35744.8$ cm^{-1} , respectively. The corresponding population and emission results are presented

in Figs. 6, 7 and 8. In Fig. 6, the remaining laser and cavity parameters are again chosen as $T = 15$ fs, $I = 5 \cdot 10^{11}$ W/cm², $g = 0.01$ au as well as $\gamma_c = 0.001$ au, $\gamma_c = 0.0025$ au, and $\gamma_c = 0.005$ au. With these parameters, the pump pulse transfers population dominantly to the photonic part of the 1UP state. We note that the current setup is related to case 2 of Ref. 71 where oscillations in the emission signal could be explained by nonadiabatic population transfer between the 1UP and 1LP states. The results shown in Fig. 6 are in line with those presented in Fig. 2. We can again observe that the non-Hermitian TDSE method is able to reproduce the emission signal and populations of excited polaritonic states with high accuracy in this particular case.

Fig. 7 reveals trends similar to those observed in Fig. 3. Here we have employed the cavity and laser parameters $g = 0.01$ au, $\gamma_c = 0.005$ au, $I = 5 \cdot 10^{11}$ W/cm² or $I = 10^{12}$ W/cm² and $T = 30$ fs. Besides the dominantly-populated 1UP state, the 2UP state also acquires some population during laser excitation. The non-Hermitian TDSE description starts to break down in Fig. 7, manifesting in visible differences between the Lindblad and TDSE populations and emissions. Indeed, the Lindblad approach again provides a much more efficient population transfer for longer pulses and higher intensities than the TDSE, which can be explained by the arguments outlined in Section III A.

The differences between the Lindblad and TDSE methods are even more prominent in Fig. 8. Here, the pulse length has been increased to $T = 45$ fs, while other parameters has been set to $g = 0.01$ au or $g = 0.02$ au, $\gamma_c = 0.005$ au and $I = 10^{12}$ W/cm². For $g = 0.02$ au (see panel c of Fig. 8) one can again notice that some population is trapped in the 1LP state, but only in the Lindblad scheme. This is due to light-induced nonadiabatic behavior of the system. The 1LP and 1UP PESs form a light-induced conical intersection (LICI) (see panel b of Fig. 1) which can serve as a funnel for rapid nonadiabatic population transfer. This effect can be hardly seen for $g = 0.01$ au, but becomes significant for $g = 0.02$ au. This finding is readily explained by the fact that light-induced nonadiabatic effects increase with the cavity coupling strength g . Time-dependent probability densities shown in Figs. 9 and 10 ($g = 0.02$ au) shed further light on the ultrafast dynamics through the LICI between the 1UP and 1LP PESs. Fig. 9 shows that although the Lindblad and TDSE probability densities have similar shapes for the 1UP and 2UP PESs ($t = 30$ fs), the TDSE probability densities have considerably smaller norms than the Lindblad ones. This observation is verified by the different scales of the z axis in Fig. 9 and it is also in line with the population curves given

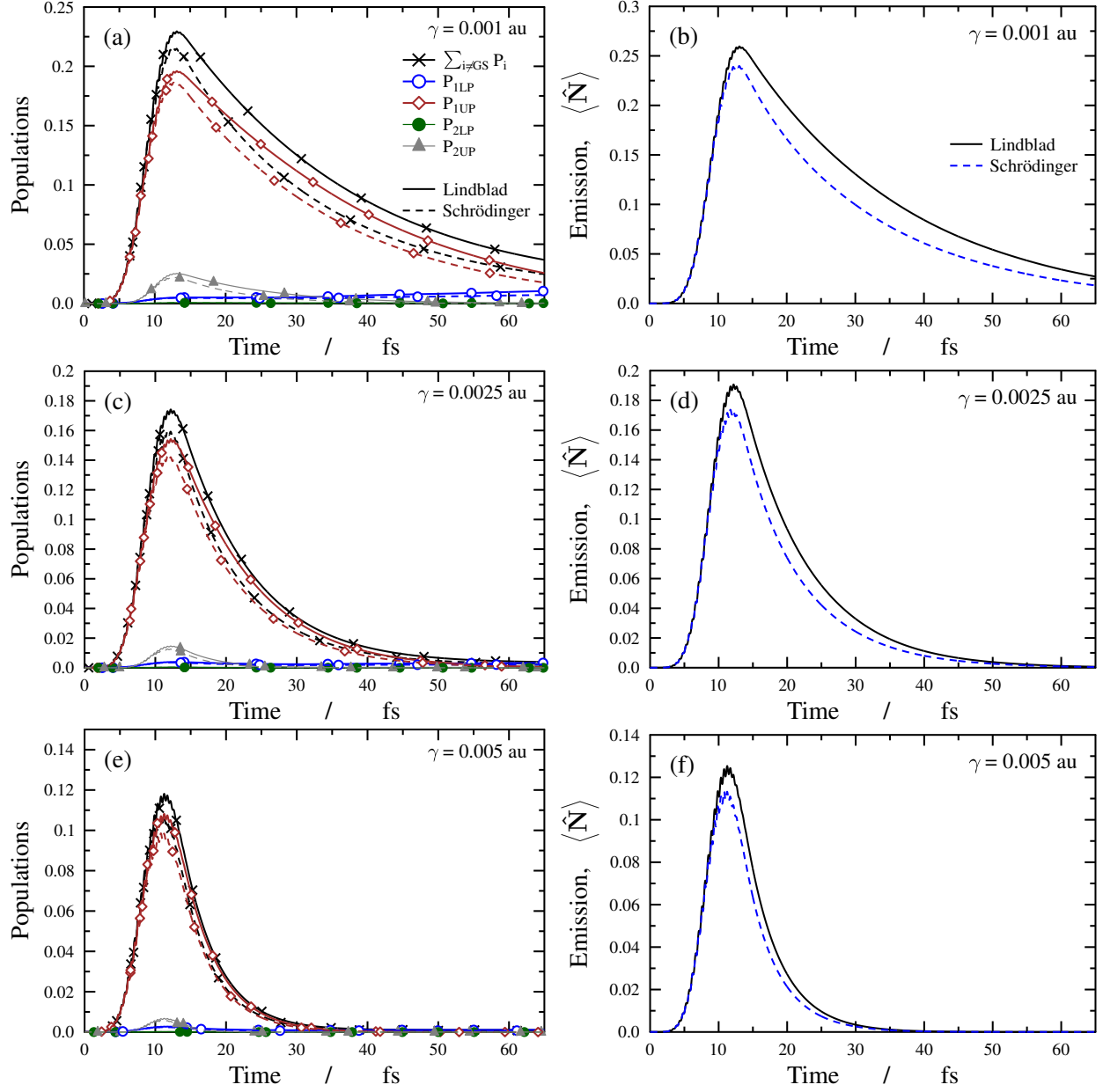


FIG. 6. Populations of polaritonic states and emission curves (the emission is proportional to the expectation value of the photon number operator \hat{N}) for cavity decay rates $\gamma_c = 0.001$ au (equivalent to a lifetime of $\tau = 24.2$ fs, panels a and b), $\gamma_c = 0.0025$ au ($\tau = 9.7$ fs, panels c and d) and $\gamma_c = 0.005$ au ($\tau = 4.8$ fs, panels e and f). The cavity wavenumber and coupling strength equal $\omega_c = 35744.8$ cm^{-1} and $g = 0.01$ au, respectively. Parameters of the pump laser pulse are chosen as $\omega = 36000$ cm^{-1} , $T = 15$ fs and $I = 5 \cdot 10^{11}$ W/cm^2 . The Lindblad results (solid lines) agree well with their Schrödinger (TDSE) counterparts (dashed lines) in all cases presented.

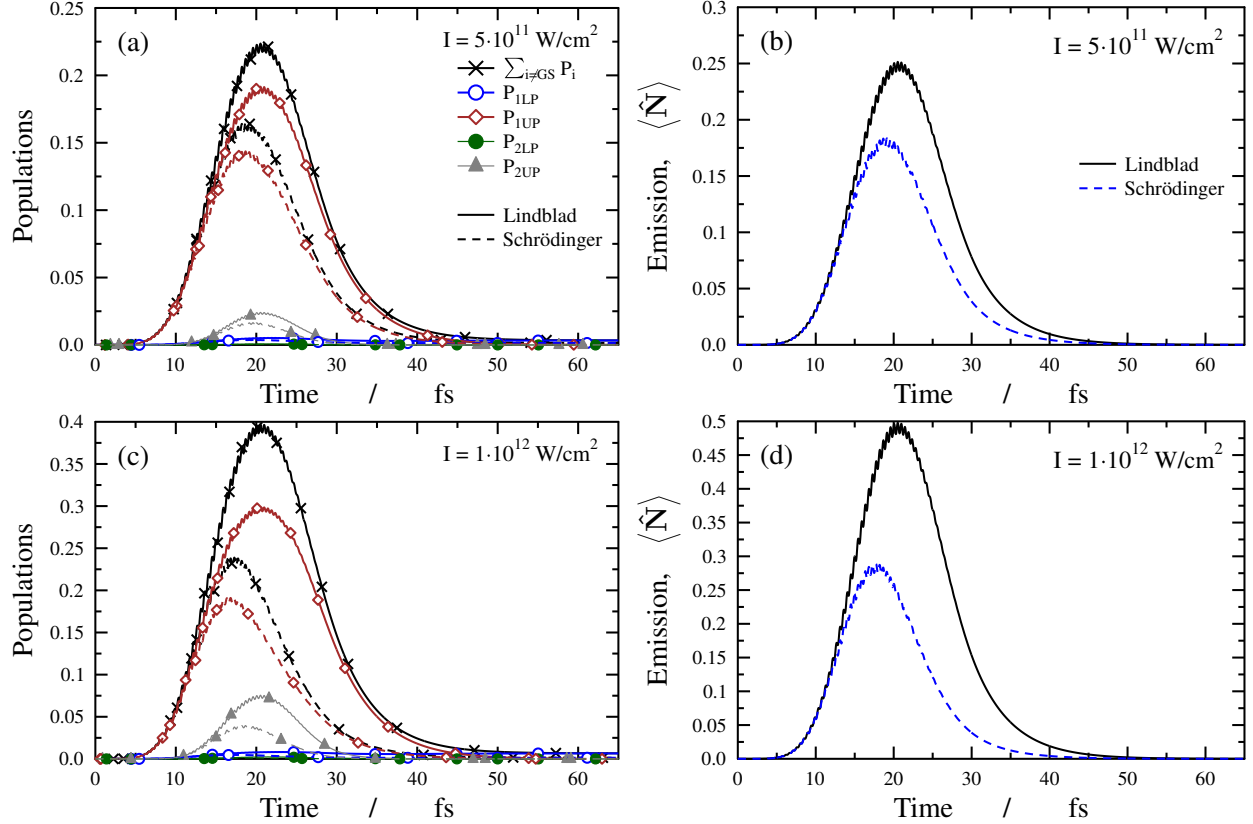


FIG. 7. Populations of polaritonic states and emission curves (the emission is proportional to the expectation value of the photon number operator \hat{N}) for laser intensities $I = 5 \cdot 10^{11} \text{ W/cm}^2$ (panels a and b) and $I = 10^{12} \text{ W/cm}^2$ (panels c and d). The cavity wavenumber and coupling strength equal $\omega_c = 35744.8 \text{ cm}^{-1}$ and $g = 0.01 \text{ au}$, respectively, while the cavity decay rate is set to $\gamma_c = 0.005 \text{ au}$ (equivalent to a lifetime of $\tau = 4.8 \text{ fs}$). Other parameters of the pump laser pulse are chosen as $\omega = 36000 \text{ cm}^{-1}$ and $T = 30 \text{ fs}$. The Lindblad results (solid lines) show visible deviations from their Schrödinger (TDSE) counterparts (dashed lines).

in Fig. 8). Turning to Fig. 10 depicting Lindblad probability densities for $t = 60 \text{ fs}$, one can clearly see that dominant part of the 1UP population is transferred to the excitonic part of the 1LP PES through the LICI, which again quenches photon emission. This is possible only for the Lindblad master equation as in the TDSE case the 1UP population does not persist until nonadiabatic population transfer can set in.

Similarly to the Section III A, we have repeated the current TDSE calculations using the renormalized TDSE method. The corresponding results are presented in Figs. 17, 19 and 21 (see Appendix A). The renormalized TDSE results show an almost perfect agreement

with their Lindblad counterparts, which is again due to the ground-state population refill induced by the renormalization of the wave function. The respective density matrix purities are depicted in Figs. 18, 20 and 22 of Appendix A. In all cases considered in this section, the purity of the density matrix equals one to a good approximation. Results for the one-photon initial state used at the end of Section III A are given in Appendix B (see panels c and d of Figs. 23 and 24 for $\omega_c = 35744.8 \text{ cm}^{-1}$). Here we can again observe the breakdown of the renormalized TDSE method, which, together with the shape of the respective purity function (see the curve labeled as UP in Fig. 25), can be understood along the lines explained at the end of Section III A.

IV. CONCLUSIONS

In this paper, the performance of the non-Hermitian time-dependent Schrödinger equation (TDSE) has been compared to that of the Lindblad-master-equation approach for lossy plasmonic nanocavities. As test system, a two-dimensional vibrational model of the four-atomic formaldehyde molecule has been used. To carry out a thorough comparison of the two methods, several different cavity and laser pumping parameters have been applied.

To summarize the findings of this paper we may say the following. (i) First of all, if the lower (1LP) and upper (1UP) polaritonic states in the singly-excited subspace are driven by a laser pulse, the TDSE with a non-Hermitian Hamiltonian (without renormalization of the wave function) is found to work well in several situations (typically for lower laser intensities and shorter pulses) concerning the excited-state populations and cavity emission signal. However, Lindblad and TDSE populations of the ground polaritonic state always differ since the TDSE method does not incorporate incoherent transitions which return population from excited polaritonic states to the ground polaritonic state. (ii) For larger laser intensities, or sufficiently long pulses (compared to the cavity photon lifetime), the TDSE results show visible or even substantial deviations from their Lindblad counterparts, even for the populations of excited polaritonic states and the cavity emission signal. A detailed analysis presented in Section III has shown that the breakdown of the non-Hermitian TDSE method can be explained by the interplay of “upward” laser excitation and “downward” incoherent transitions. (iii) It is eye-catching that for all cases studied, the TDSE reproduces excellently all populations and emission signals for short times. (iv) We have also demonstrated that

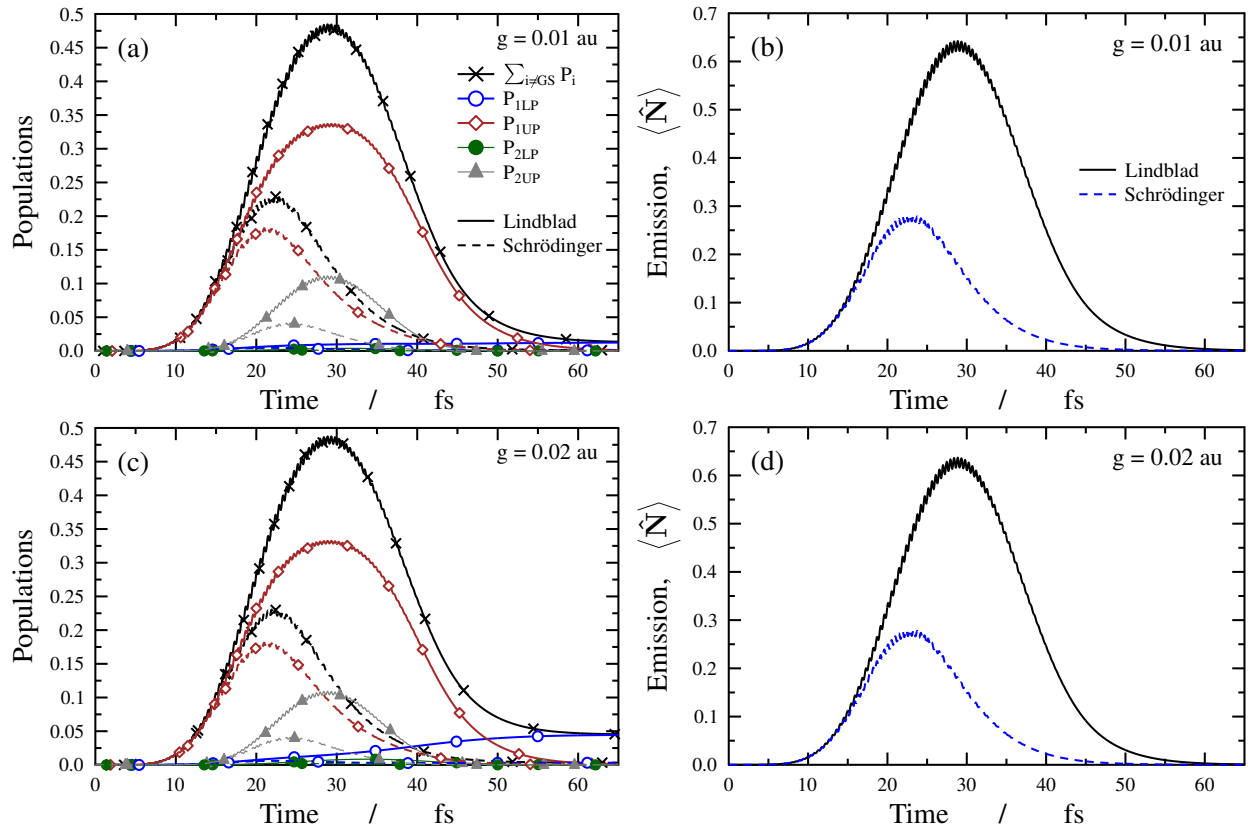


FIG. 8. Populations of polaritonic states and emission curves (the emission is proportional to the expectation value of the photon number operator \hat{N}) for coupling strength values of $g = 0.01$ au (panels a and b) and $g = 0.02$ au (panels c and d). The cavity wavenumber and decay rate equal $\omega_c = 35744.8$ cm^{-1} and $\gamma_c = 0.005$ au (equivalent to a lifetime of $\tau = 4.8$ fs), respectively. Parameters of the pump laser pulse are chosen as $\omega = 36000$ cm^{-1} , $T = 45$ fs and $I = 10^{12}$ W/cm^2 . The Lindblad results (solid lines) differ substantially from their Schrödinger (TDSE) counterparts (dashed lines).

the discrepancies between the Lindblad and non-Hermitian TDSE results can be greatly reduced by renormalizing the wave function at each time step during the numerical solution of the TDSE.

An important advantage of the non-Hermitian TDSE is that it enables the inclusion of many more nuclear degrees of freedom (rotational and vibrational) in the quantum-dynamical description due to its lower computational cost compared to the Lindblad master equation. Thus, the non-Hermitian TDSE, in the appropriate range of parameters (and also in combination with wave function renormalization), can also offer a correct treatment of

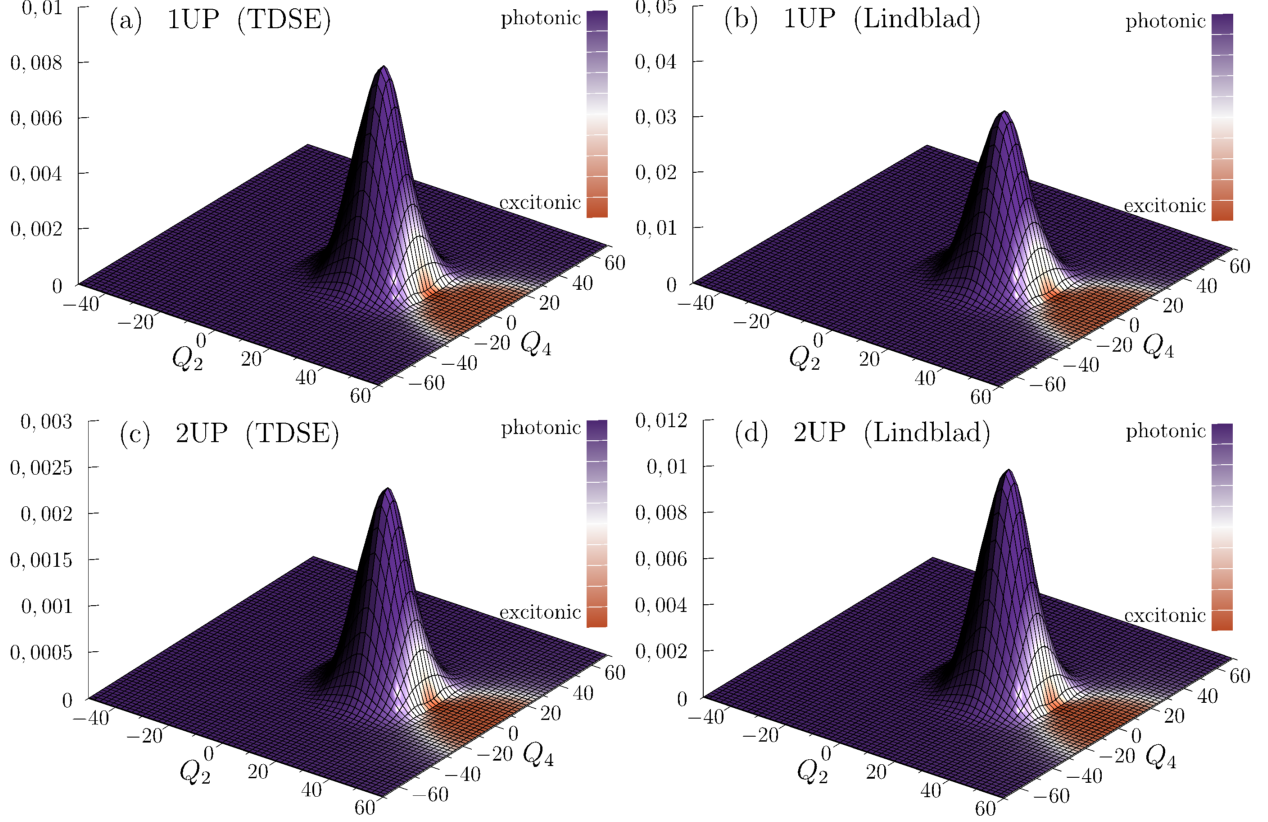


FIG. 9. Probability density figures (obtained with the Lindblad and Schrödinger (TDSE) equations) at $t = 30$ fs for the 1UP (upper polaritonic, panels a and b) and 2UP (panels c and d) potential energy surfaces. The cavity wavenumber, coupling strength and decay rate equal $\omega_c = 35744.8 \text{ cm}^{-1}$, $g = 0.02 \text{ au}$ and $\gamma_c = 0.005 \text{ au}$, respectively. Parameters of the pump laser pulse are chosen as $\omega = 36000 \text{ cm}^{-1}$, $T = 45 \text{ fs}$ and $I = 10^{12} \text{ W/cm}^2$. The laser pulse populates mainly the 1UP and 2UP states and the wave packet is localized in the photonic (purple) region in all cases. Although the Lindblad and Schrödinger probability densities have similar shapes, the norm of the Schrödinger probability densities are definitely smaller than those of the Lindblad probability densities (see the different scales along the z axis).

light-induced nonadiabatic properties of small diatomic molecules in a lossy nanocavity.

ACKNOWLEDGMENTS

The authors are indebted to NKFIH for funding (Grants No. K146096 and K138233). Financial support by the Deutsche Forschungsgemeinschaft (DFG) (Grant No. CE 10/56-1) is

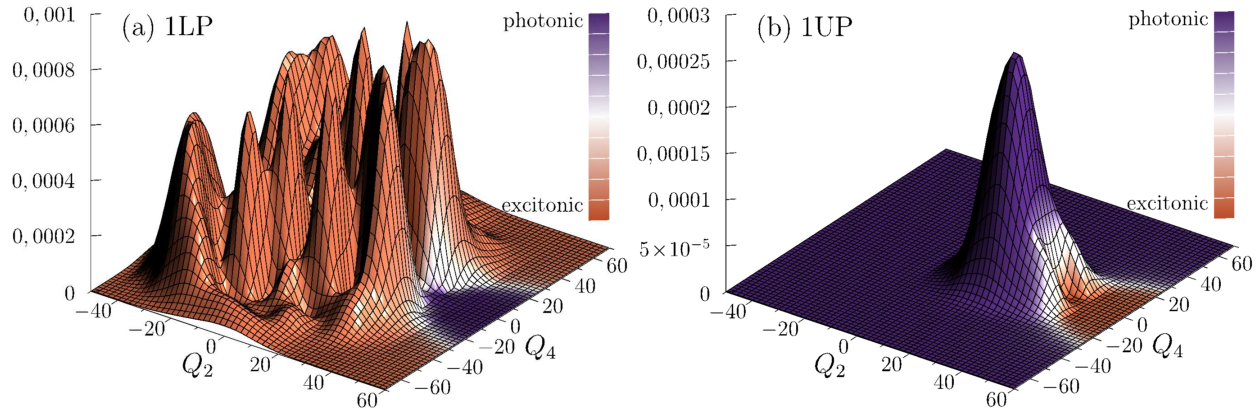


FIG. 10. Probability density figures (obtained with the Lindblad equation) at $t = 60$ fs for the 1LP (lower polaritonic, panel a) and 1UP (upper polaritonic, panel b) potential energy surfaces. The cavity wavenumber, coupling strength and decay rate equal $\omega_c = 35744.8 \text{ cm}^{-1}$, $g = 0.02 \text{ au}$ and $\gamma_c = 0.005 \text{ au}$, respectively. Parameters of the pump laser pulse are chosen as $\omega = 36000 \text{ cm}^{-1}$, $T = 45 \text{ fs}$ and $I = 10^{12} \text{ W/cm}^2$. One can observe nonadiabatic population transfer from the photonic (purple) region of the initially-populated 1UP state to the excitonic (orange) region of the 1LP state.

gratefully acknowledged. The work performed in Budapest received funding from the HUNREN Hungarian Research Network. This publication supports research performed within the COST Actions CA21101 “Confined molecular systems: from a new generation of materials to the stars” (COSY), and CA18222 “Attosecond Chemistry” (AttoChem), funded by the European Cooperation in Science and Technology (COST), and the PHYMOL (Physics, Accuracy and Machine Learning: Towards the Next Generation of Molecular Potentials) project, funded mainly under the Horizon Europe scheme.

DATA AVAILABILITY

The data that support the findings of this study are available from the corresponding author upon reasonable request.

CONFLICTS OF INTEREST

The authors have no conflicts to disclose.

Appendix A: Renormalized Schrödinger (TDSE) results and density matrix purities

Figs. 11, 13, 15 and Figs. 17, 19 and 21 show population and emission results obtained with the Lindblad and renormalized TDSE methods using the parameters of Section III A and Section III B, respectively. The corresponding density matrix purities ($\text{tr}(\hat{\rho}^2)$) are depicted in Figs. 12, 14, 16 and Figs. 18, 20, 22. In all cases, the Lindblad results show an excellent agreement with their counterparts obtained with the renormalized TDSE method. Moreover, the purities equal one at $t = 0$ and remain close to one for all times shown in the figures.

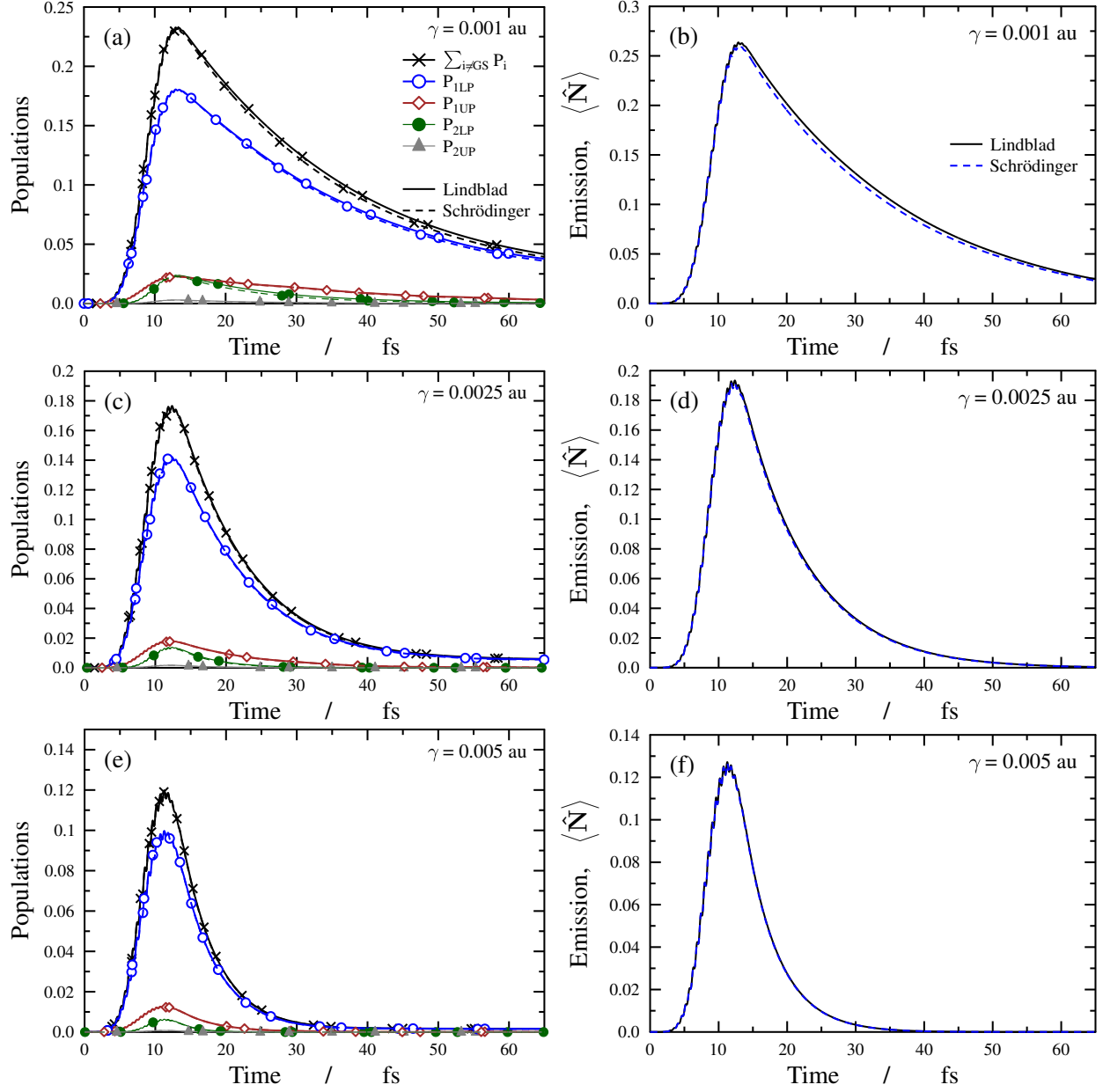


FIG. 11. Populations of polaritonic states and emission curves (the emission is proportional to the expectation value of the photon number operator \hat{N}) for cavity decay rates $\gamma_c = 0.001$ au (equivalent to a lifetime of $\tau = 24.2$ fs, panels a and b), $\gamma_c = 0.0025$ au ($\tau = 9.7$ fs, panels c and d) and $\gamma_c = 0.005$ au ($\tau = 4.8$ fs, panels e and f). The Lindblad and renormalized Schrödinger (TDSE) results are depicted by solid and dashed lines, respectively. The cavity wavenumber and coupling strength equal $\omega_c = 29957.2$ cm^{-1} and $g = 0.01$ au, respectively. Parameters of the pump laser pulse are chosen as $\omega = 30000$ cm^{-1} , $T = 15$ fs and $I = 5 \cdot 10^{11}$ W/cm^2 .

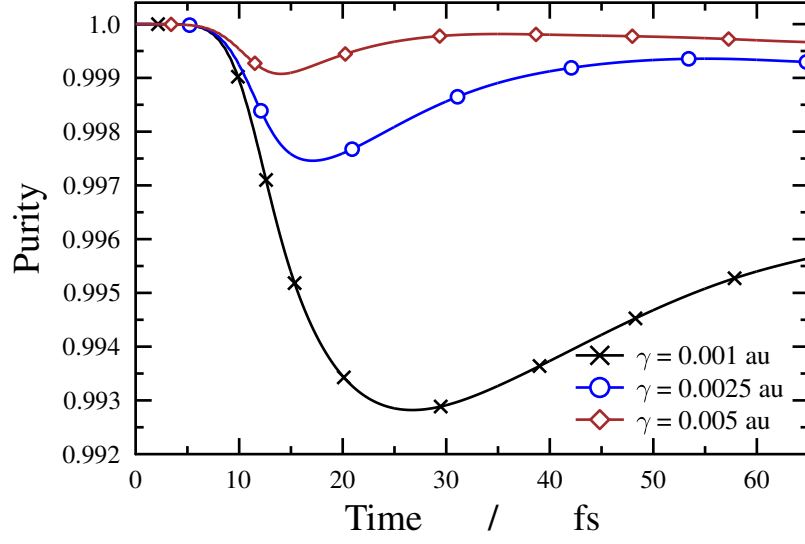


FIG. 12. Purity of the density matrix ($\text{tr}(\hat{\rho}^2)$) as a function of time for cavity decay rates $\gamma_c = 0.001$ au, $\gamma_c = 0.0025$ au and $\gamma_c = 0.005$ au. Unspecified cavity and laser parameters correspond to those applied in Figs. 2 and 11.

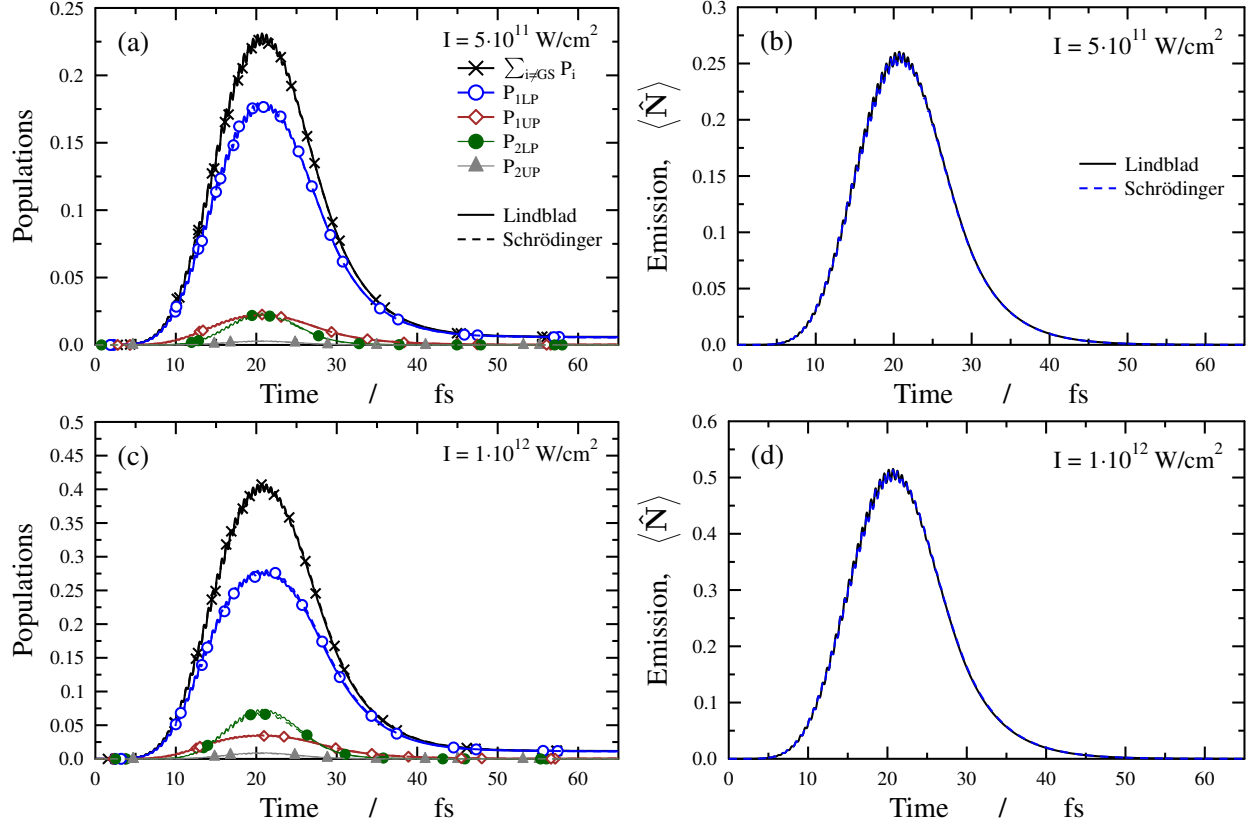


FIG. 13. Populations of polaritonic states and emission curves (the emission is proportional to the expectation value of the photon number operator \hat{N}) for laser intensities $I = 5 \cdot 10^{11} \text{ W/cm}^2$ (panels a and b) and $I = 10^{12} \text{ W/cm}^2$ (panels c and d). The Lindblad and renormalized Schrödinger (TDSE) results are depicted by solid and dashed lines, respectively. The cavity wavenumber and coupling strength equal $\omega_c = 29957.2 \text{ cm}^{-1}$ and $g = 0.01 \text{ au}$, respectively, while the cavity decay rate is set to $\gamma_c = 0.005 \text{ au}$ (equivalent to a lifetime of $\tau = 4.8 \text{ fs}$). Other parameters of the pump laser pulse are chosen as $\omega = 30000 \text{ cm}^{-1}$ and $T = 30 \text{ fs}$.

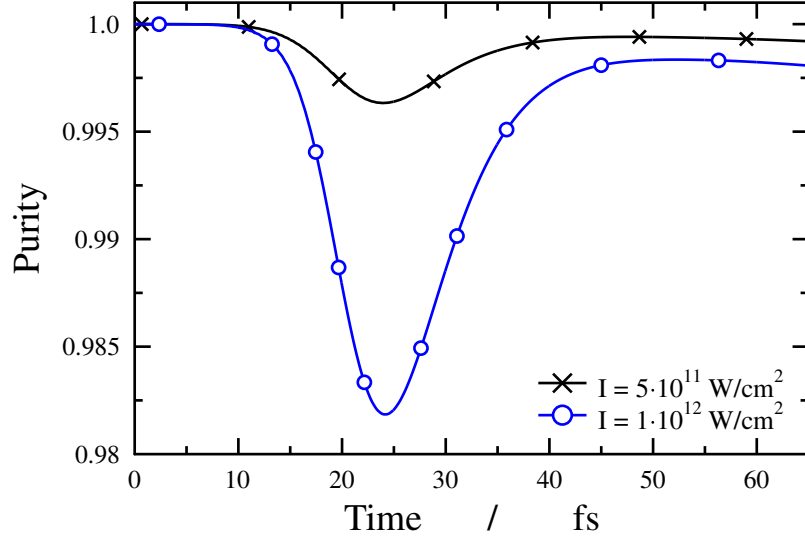


FIG. 14. Purity of the density matrix ($\text{tr}(\hat{\rho}^2)$) as a function of time for laser intensities $I = 5 \cdot 10^{11} \text{ W/cm}^2$ and $I = 10^{12} \text{ W/cm}^2$. Unspecified cavity and laser parameters correspond to those applied in Figs. 3 and 13.

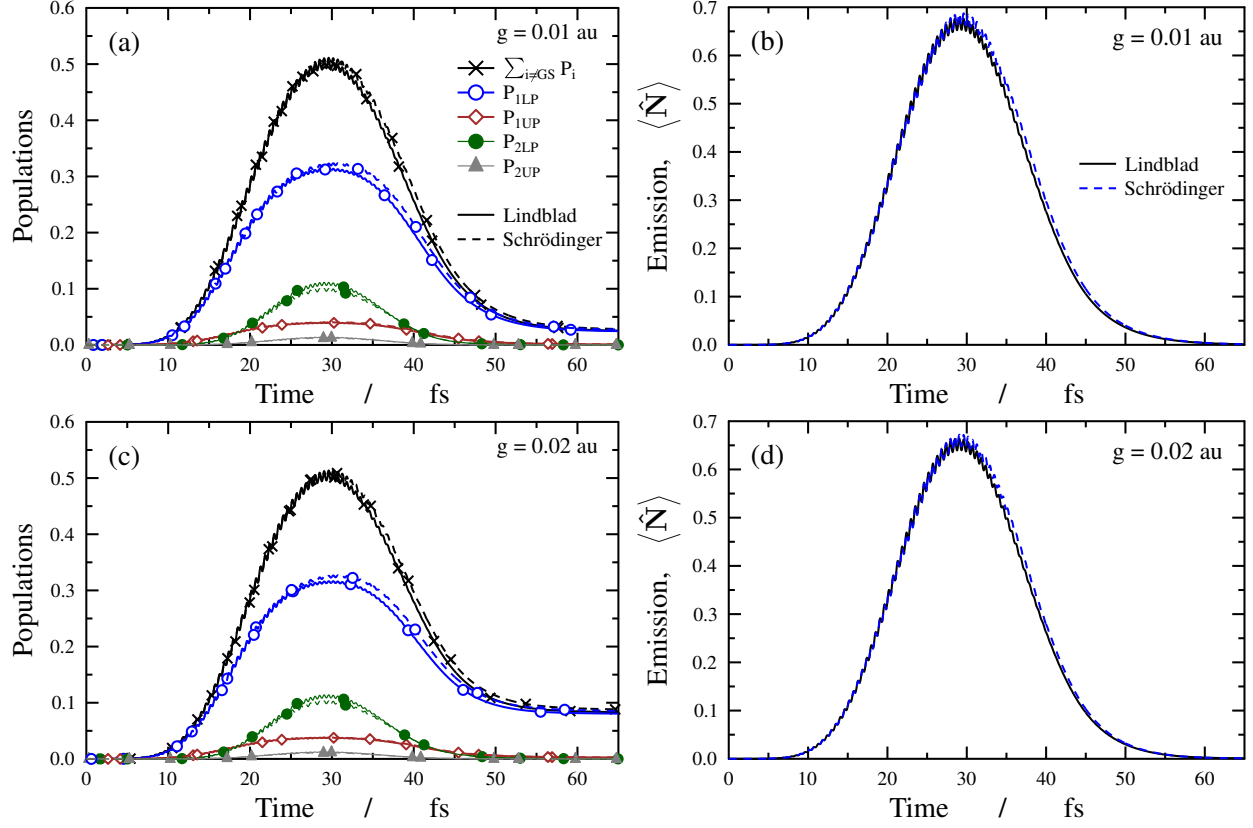


FIG. 15. Populations of polaritonic states and emission curves (the emission is proportional to the expectation value of the photon number operator \hat{N}) for coupling strength values of $g = 0.01$ au (panels a and b) and $g = 0.02$ au (panels c and d). The Lindblad and renormalized Schrödinger (TDSE) results are depicted by solid and dashed lines, respectively. The cavity wavenumber and decay rate equal $\omega_c = 29957.2 \text{ cm}^{-1}$ and $\gamma_c = 0.005$ au (equivalent to a lifetime of $\tau = 4.8$ fs), respectively. Parameters of the pump laser pulse are chosen as $\omega = 30000 \text{ cm}^{-1}$, $T = 45$ fs and $I = 10^{12} \text{ W/cm}^2$.

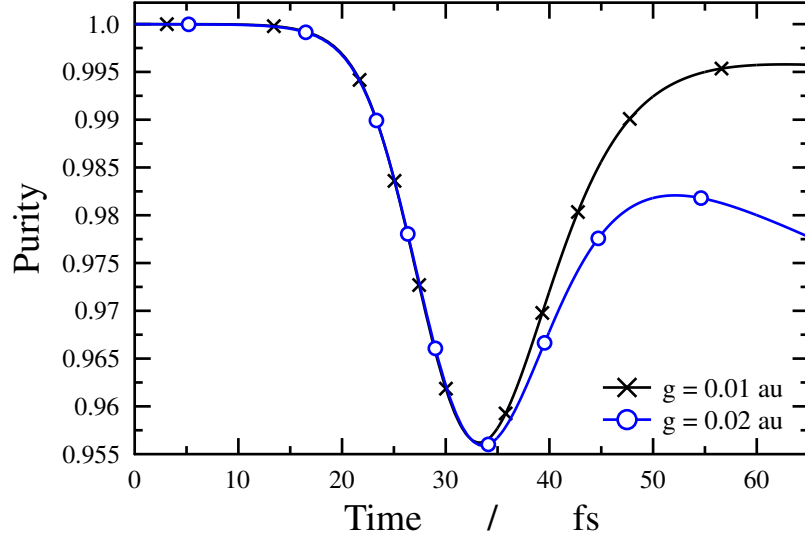


FIG. 16. Purity of the density matrix ($\text{tr}(\hat{\rho}^2)$) as a function of time for coupling strength values of $g = 0.01$ au and $g = 0.02$ au. Unspecified cavity and laser parameters correspond to those applied in Figs. 4 and 15.

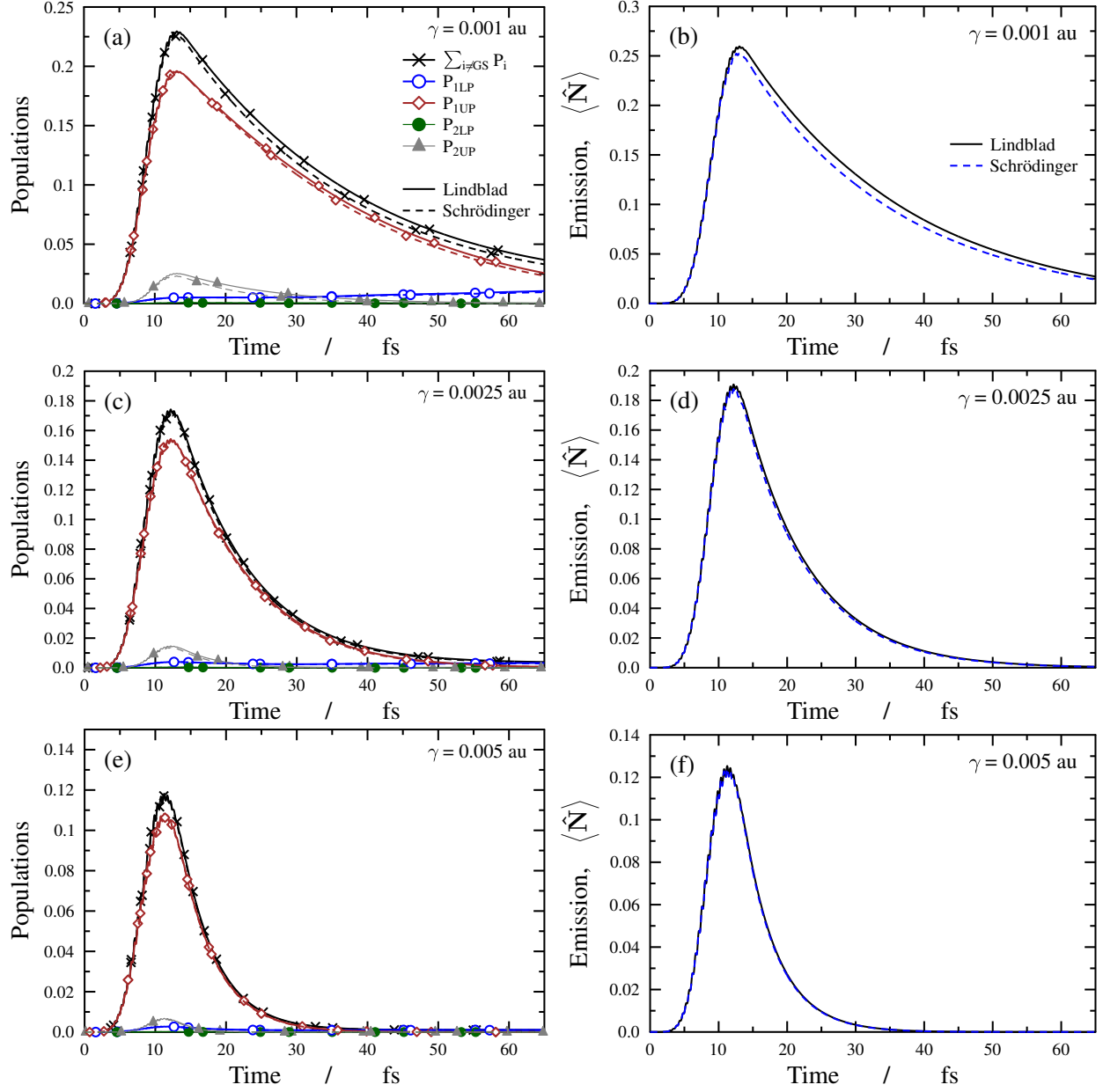


FIG. 17. Populations of polaritonic states and emission curves (the emission is proportional to the expectation value of the photon number operator \hat{N}) for cavity decay rates $\gamma_c = 0.001$ au (equivalent to a lifetime of $\tau = 24.2$ fs, panels a and b), $\gamma_c = 0.0025$ au ($\tau = 9.7$ fs, panels c and d) and $\gamma_c = 0.005$ au ($\tau = 4.8$ fs, panels e and f). The Lindblad and renormalized Schrödinger (TDSE) results are depicted by solid and dashed lines, respectively. The cavity wavenumber and coupling strength equal $\omega_c = 35744.8$ cm^{-1} and $g = 0.01$ au, respectively. Parameters of the pump laser pulse are chosen as $\omega = 36000$ cm^{-1} , $T = 15$ fs and $I = 5 \cdot 10^{11}$ W/cm^2 .

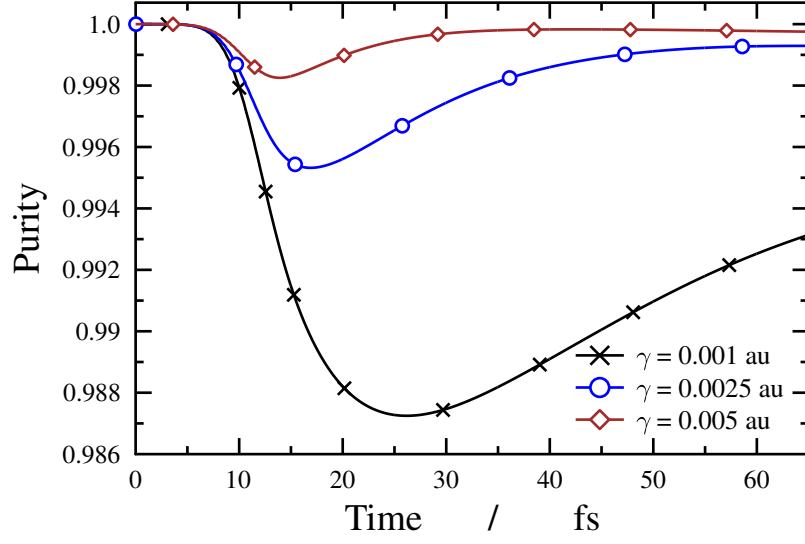


FIG. 18. Purity of the density matrix ($\text{tr}(\hat{\rho}^2)$) as a function of time for cavity decay rates $\gamma_c = 0.001$ au, $\gamma_c = 0.0025$ au and $\gamma_c = 0.005$ au. Unspecified cavity and laser parameters correspond to those applied in Figs. 6 and 17.

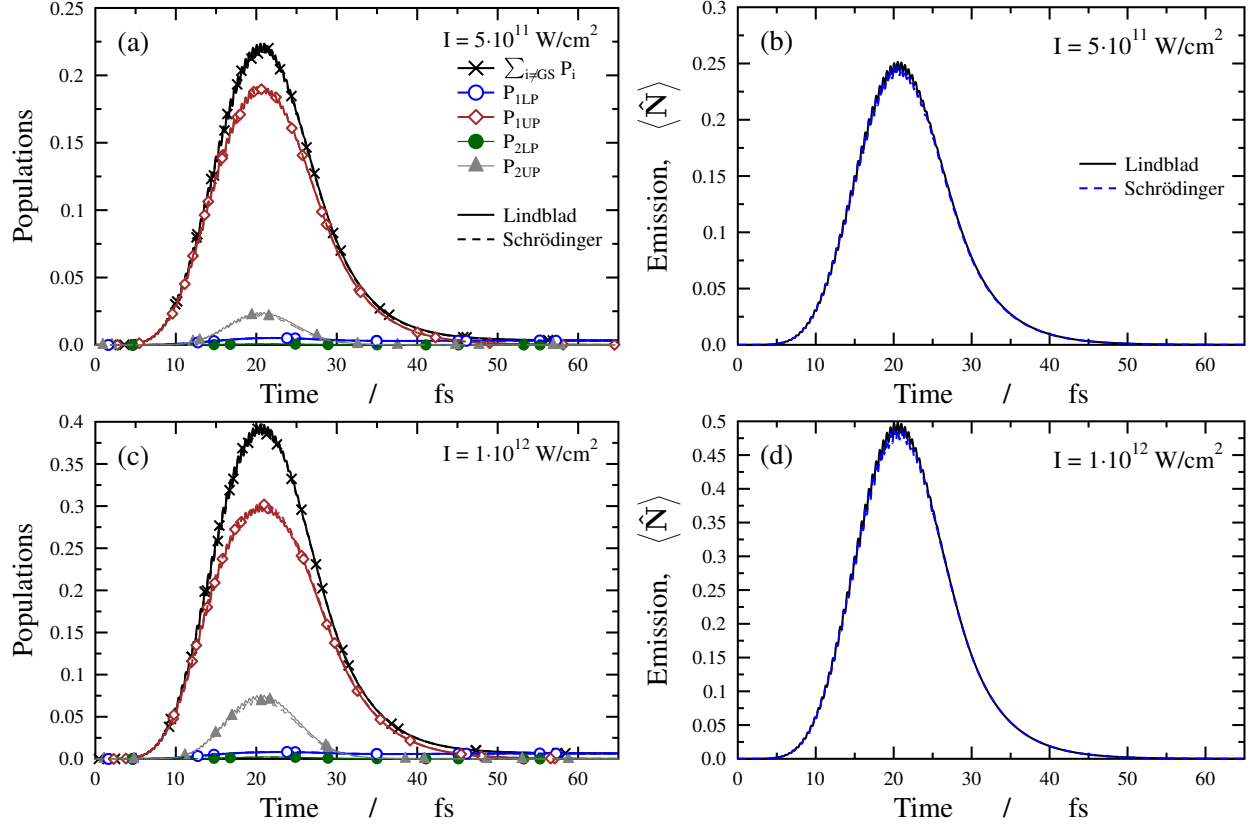


FIG. 19. Populations of polaritonic states and emission curves (the emission is proportional to the expectation value of the photon number operator \hat{N}) for laser intensities $I = 5 \cdot 10^{11} \text{ W/cm}^2$ (panels a and b) and $I = 10^{12} \text{ W/cm}^2$ (panels c and d). The Lindblad and renormalized Schrödinger (TDSE) results are depicted by solid and dashed lines, respectively. The cavity wavenumber and coupling strength equal $\omega_c = 35744.8 \text{ cm}^{-1}$ and $g = 0.01 \text{ au}$, respectively, while the cavity decay rate is set to $\gamma_c = 0.005 \text{ au}$ (equivalent to a lifetime of $\tau = 4.8 \text{ fs}$). Other parameters of the pump laser pulse are chosen as $\omega = 36000 \text{ cm}^{-1}$ and $T = 30 \text{ fs}$.

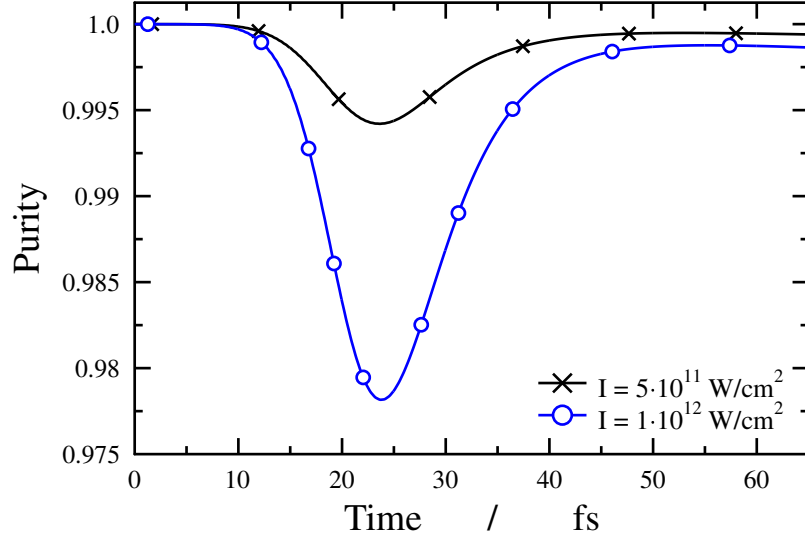


FIG. 20. Purity of the density matrix ($\text{tr}(\hat{\rho}^2)$) as a function of time for laser intensities $I = 5 \cdot 10^{11} \text{ W/cm}^2$ and $I = 10^{12} \text{ W/cm}^2$. Unspecified cavity and laser parameters correspond to those applied in Figs. 7 and 19.

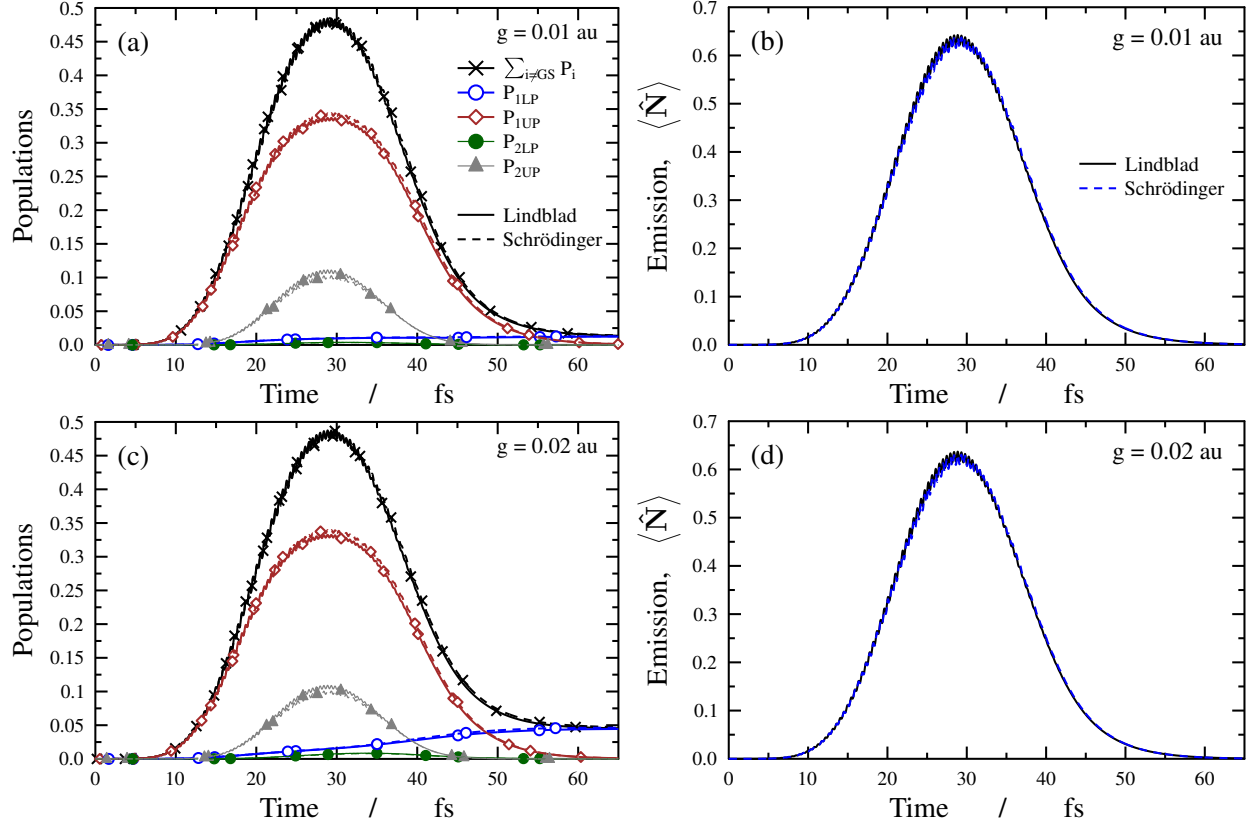


FIG. 21. Populations of polaritonic states and emission curves (the emission is proportional to the expectation value of the photon number operator \hat{N}) for coupling strength values of $g = 0.01$ au (panels a and b) and $g = 0.02$ au (panels c and d). The Lindblad and renormalized Schrödinger (TDSE) results are depicted by solid and dashed lines, respectively. The cavity wavenumber and decay rate equal $\omega_c = 35744.8 \text{ cm}^{-1}$ and $\gamma_c = 0.005$ au (equivalent to a lifetime of $\tau = 4.8$ fs), respectively. Parameters of the pump laser pulse are chosen as $\omega = 36000 \text{ cm}^{-1}$, $T = 45$ fs and $I = 10^{12} \text{ W/cm}^2$.

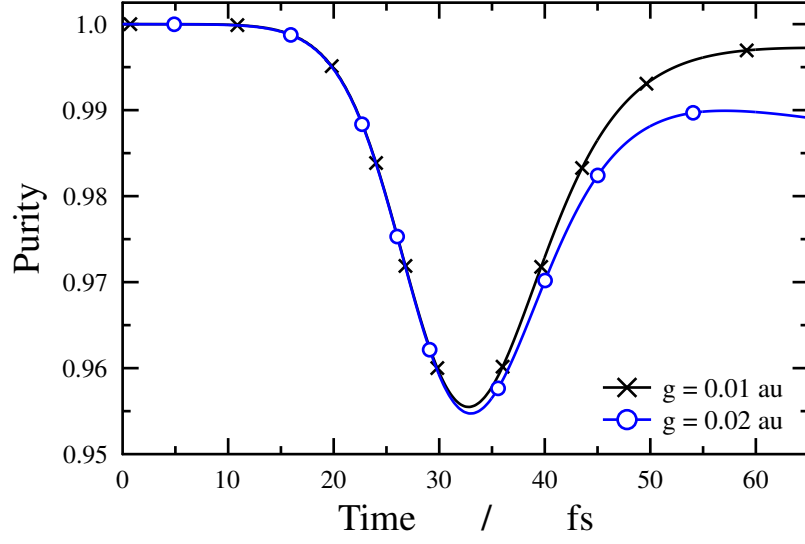


FIG. 22. Purity of the density matrix ($\text{tr}(\hat{\rho}^2)$) as a function of time for coupling strength values of $g = 0.01$ au and $g = 0.02$ au. Unspecified cavity and laser parameters correspond to those applied in Figs. 8 and 21.

Appendix B: Reference results with a special initial state

This section presents results with a special initial state, that is, the molecule is in the vibrational ground state of the ground electronic state and there is 1 photon in the cavity mode at $t = 0$. Fig. 23 compares populations of polaritonic states and emission curves obtained with the Lindblad and non-Hermitian TDSE methods, showing good agreement for both cavity wavenumbers ($\omega_c = 29957.2 \text{ cm}^{-1}$ and $\omega_c = 35744.8 \text{ cm}^{-1}$). The same results are depicted in Fig. 24 for the Lindblad and renormalized TDSE methods which show substantial deviations for both cavity wavenumbers in this particular case. Finally, Fig. 25 presents purity results. In all figures, the coupling strength and cavity decay rate are set to $g = 0.01 \text{ au}$ and $\gamma_c = 0.001 \text{ au}$, respectively.

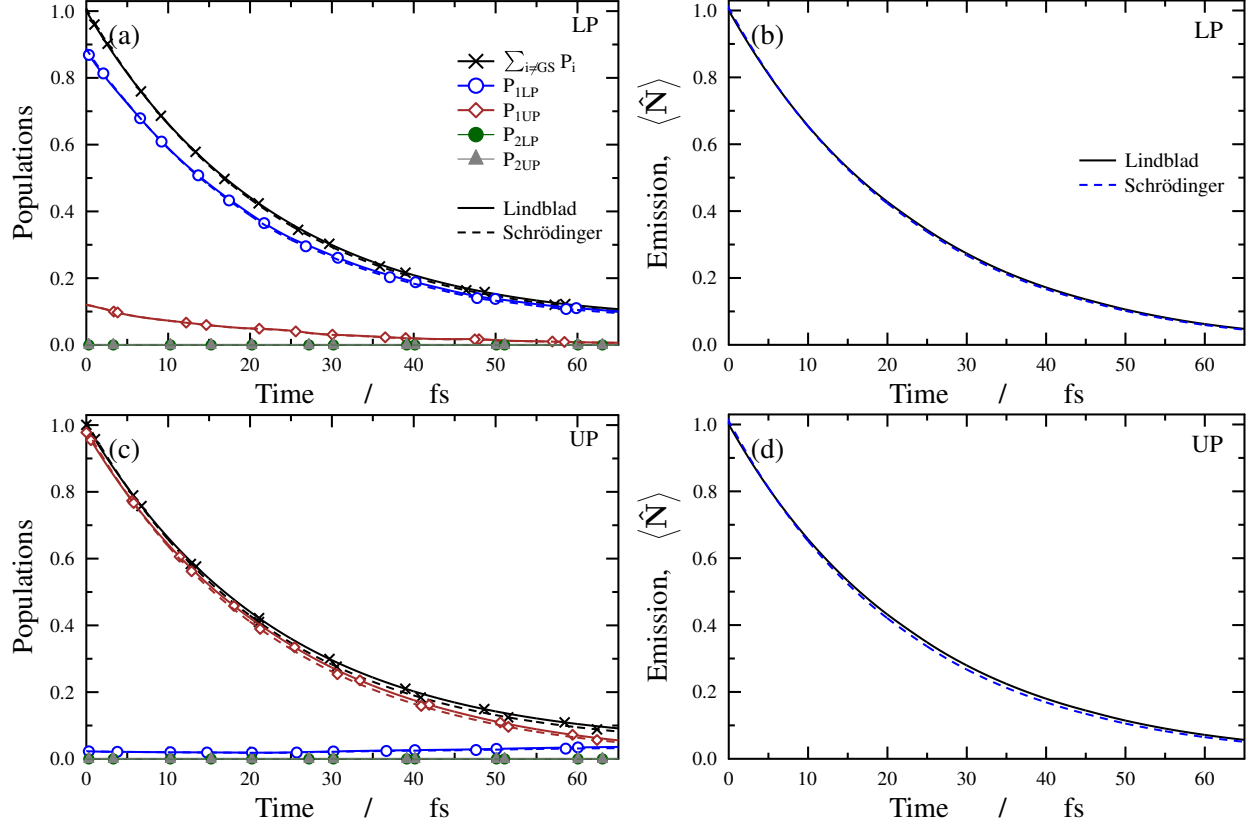


FIG. 23. Populations of polaritonic states and emission curves (the emission is proportional to the expectation value of the photon number operator \hat{N}). The initial state is chosen as follows: molecule in the vibrational ground state of the ground (X) electronic state with 1 photon in the cavity mode. The Lindblad and Schrödinger (TDSE) results are depicted by solid and dashed lines, respectively. The cavity wavenumber is set to $\omega_c = 29957.2 \text{ cm}^{-1}$ (panels a and b) or $\omega_c = 35744.8 \text{ cm}^{-1}$ (panels c and d). The coupling strength and cavity decay rate equal $g = 0.01 \text{ au}$ and $\gamma_c = 0.001 \text{ au}$, respectively.

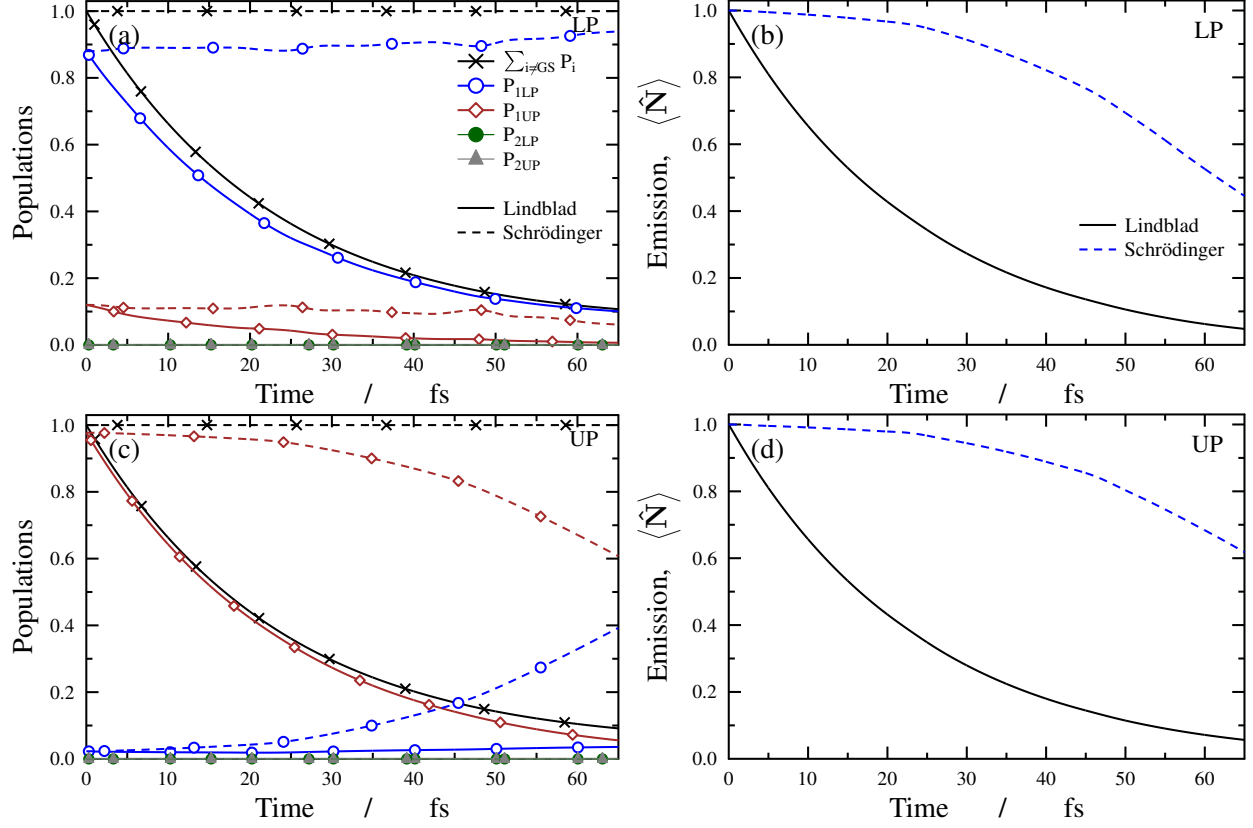


FIG. 24. Populations of polaritonic states and emission curves (the emission is proportional to the expectation value of the photon number operator \hat{N}). The initial state is chosen as follows: molecule in the vibrational ground state of the ground (X) electronic state with 1 photon in the cavity mode. The Lindblad and renormalized Schrödinger (TDSE) results are depicted by solid and dashed lines, respectively. The cavity wavenumber is set to $\omega_c = 29957.2 \text{ cm}^{-1}$ (panels a and b) or $\omega_c = 35744.8 \text{ cm}^{-1}$ (panels c and d). The coupling strength and cavity decay rate equal $g = 0.01 \text{ au}$ and $\gamma_c = 0.001 \text{ au}$, respectively.

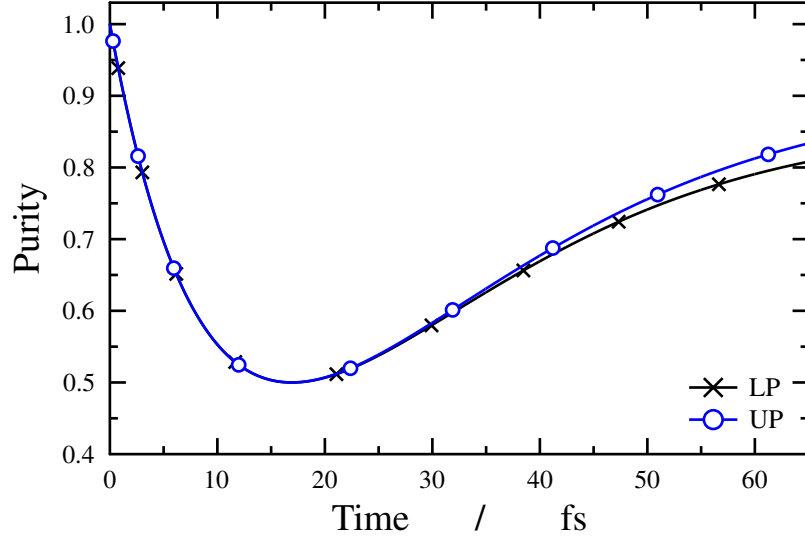


FIG. 25. Purity of the density matrix ($\text{tr}(\hat{\rho}^2)$) as a function of time for the initial state used in Figs. 23 and 24. The cavity wavenumber is set to $\omega_c = 29957.2 \text{ cm}^{-1}$ (labeled as LP) or $\omega_c = 35744.8 \text{ cm}^{-1}$ (UP). The coupling strength and cavity decay rate equal $g = 0.01 \text{ au}$ and $\gamma_c = 0.001 \text{ au}$, respectively.

REFERENCES

- ¹P. Törmä and W. L. Barnes, “Strong coupling between surface plasmon polaritons and emitters: a review,” *Rep. Prog. Phys.* **78**, 013901 (2015).
- ²J. A. Hutchison, T. Schwartz, C. Genet, E. Devaux, and T. W. Ebbesen, “Modifying chemical landscapes by coupling to vacuum fields,” *Angew. Chem. Int. Ed.* **51**, 1592–1596 (2012).
- ³T. W. Ebbesen, “Hybrid light–matter states in a molecular and material science perspective,” *Acc. Chem. Res.* **49**, 2403–2412 (2016).
- ⁴A. Thomas, J. George, A. Shalabney, M. Dryzhakov, S. J. Varma, J. Moran, T. Chervy, X. Zhong, E. Devaux, C. Genet, J. A. Hutchison, and T. W. Ebbesen, “Ground-state chemical reactivity under vibrational coupling to the vacuum electromagnetic field,” *Angew. Chem. Int. Ed.* **55**, 11462–11466 (2016).
- ⁵R. M. A. Vergauwe, J. George, T. Chervy, J. A. Hutchison, A. Shalabney, V. Y. Torbeev, and T. W. Ebbesen, “Quantum strong coupling with protein vibrational modes,” *J. Phys. Chem. Lett.* **7**, 4159–4164 (2016).
- ⁶X. Zhong, T. Chervy, S. Wang, J. George, A. Thomas, J. A. Hutchison, E. Devaux, C. Genet, and T. W. Ebbesen, “Non-radiative energy transfer mediated by hybrid light-matter states,” *Angew. Chem.* **128**, 6310–6314 (2016).
- ⁷R. Chikkaraddy, B. de Nijs, F. Benz, S. J. Barrow, O. A. Scherman, E. Rosta, A. Demetriadou, P. Fox, O. Hess, and J. J. Baumberg, “Single-molecule strong coupling at room temperature in plasmonic nanocavities,” *Nature* **535**, 127–130 (2016).
- ⁸O. Ojambati, R. Chikkaraddy, W. Deacon, M. Horton, D. Kos, V. Turek, U. Keyser, and J. Baumberg, “Quantum electrodynamics at room temperature coupling a single vibrating molecule with a plasmonic nanocavity,” *Nat. Commun.* **10**, 1049 (2019).
- ⁹T. P. Rossi, T. Shegai, P. Erhart, and T. J. Antosiewicz, “Strong plasmon-molecule coupling at the nanoscale revealed by first-principles modeling,” *Nat. Commun.* **10**, 3336 (2019).
- ¹⁰A. Thomas, L. Lethuillier-Karl, K. Nagarajan, R. M. A. Vergauwe, J. George, T. Chervy, A. Shalabney, E. Devaux, C. Genet, J. Moran, and T. W. Ebbesen, “Tilting a ground-state reactivity landscape by vibrational strong coupling,” *Science* **363**, 615–619 (2019).

- ¹¹R. M. A. Vergauwe, A. Thomas, K. Nagarajan, A. Shalabney, J. George, T. Chervy, M. Seidel, E. Devaux, V. Torbeev, and T. W. Ebbesen, “Modification of enzyme activity by vibrational strong coupling of water,” *Angew. Chem. Int. Ed.* **58**, 15324–15328 (2019).
- ¹²J. Galego, F. J. Garcia-Vidal, and J. Feist, “Cavity-induced modifications of molecular structure in the strong-coupling regime,” *Phys. Rev. X* **5**, 041022 (2015).
- ¹³M. Kowalewski, K. Bennett, and S. Mukamel, “Cavity femtochemistry: Manipulating nonadiabatic dynamics at avoided crossings,” *J. Phys. Chem. Lett.* **7**, 2050–2054 (2016).
- ¹⁴J. Feist, J. Galego, and F. J. Garcia-Vidal, “Polaritonic chemistry with organic molecules,” *ACS Photonics* **5**, 205–216 (2018).
- ¹⁵J. Flick, N. Rivera, and P. Narang, “Strong light-matter coupling in quantum chemistry and quantum photonics,” *Nanophotonics* **7**, 1479–1501 (2018).
- ¹⁶R. F. Ribeiro, L. A. Martínez-Martínez, M. Du, J. Campos-Gonzalez-Angulo, and J. Yuen-Zhou, “Polariton chemistry: controlling molecular dynamics with optical cavities,” *Chem. Sci.* **9**, 6325–6339 (2018).
- ¹⁷M. Ruggenthaler, N. Tancogne-Dejean, J. Flick, H. Appel, and A. Rubio, “From a quantum-electrodynamical light–matter description to novel spectroscopies,” *Nat. Rev. Chem.* **2**, 0118 (2018).
- ¹⁸T. Szidarovszky, G. J. Halász, A. G. Császár, L. S. Cederbaum, and Á. Vibók, “Conical intersections induced by quantum light: Field-dressed spectra from the weak to the ultrastrong coupling regimes,” *J. Phys. Chem. Lett.* **9**, 6215–6223 (2018).
- ¹⁹J. F. Triana, D. Peláez, and J. L. Sanz-Vicario, “Entangled photonic-nuclear molecular dynamics of LiF in quantum optical cavities,” *J. Phys. Chem. A* **122**, 2266–2278 (2018).
- ²⁰O. Vendrell, “Collective Jahn-Teller interactions through light-matter coupling in a cavity,” *Phys. Rev. Lett.* **121**, 253001 (2018).
- ²¹A. Csehi, M. Kowalewski, G. J. Halász, and Á. Vibók, “Ultrafast dynamics in the vicinity of quantum light-induced conical intersections,” *New J. Phys.* **21**, 093040 (2019).
- ²²A. Csehi, Á. Vibók, G. J. Halász, and M. Kowalewski, “Quantum control with quantum light of molecular nonadiabaticity,” *Phys. Rev. A* **100**, 053421 (2019).
- ²³S. Kéna-Cohen and J. Yuen-Zhou, “Polariton chemistry: Action in the dark,” *ACS Cent. Sci.* **5**, 386–388 (2019).
- ²⁴A. Mandal and P. Huo, “Investigating new reactivities enabled by polariton photochemistry,” *J. Phys. Chem. Lett.* **10**, 5519–5529 (2019).

- ²⁵J. F. Triana and J. L. Sanz-Vicario, “Revealing the presence of potential crossings in diatomics induced by quantum cavity radiation,” *Phys. Rev. Lett.* **122**, 063603 (2019).
- ²⁶C. Fábri, B. Lasorne, G. J. Halász, L. S. Cederbaum, and Á. Vibók, “Quantum light-induced nonadiabatic phenomena in the absorption spectrum of formaldehyde: Full- and reduced-dimensionality studies,” *J. Chem. Phys.* **153**, 234302 (2020).
- ²⁷J. Fregoni, S. Corni, M. Persico, and G. Granucci, “Photochemistry in the strong coupling regime: A trajectory surface hopping scheme,” *J. Comput. Chem.* **41**, 2033–2044 (2020).
- ²⁸F. Herrera and J. Owrutsky, “Molecular polaritons for controlling chemistry with quantum optics,” *J. Chem. Phys.* **152**, 100902 (2020).
- ²⁹A. Mandal, S. Montillo Vega, and P. Huo, “Polarized Fock states and the dynamical Casimir effect in molecular cavity quantum electrodynamics,” *J. Phys. Chem. Lett.* **11**, 9215–9223 (2020).
- ³⁰R. Silva, J. Pino, F. García-Vidal, and J. Feist, “Polaritonic molecular clock for all-optical ultrafast imaging of wavepacket dynamics without probe pulses,” *Nat. Commun.* **11**, 1423 (2020).
- ³¹D. Sidler, C. Schäfer, M. Ruggenthaler, and A. Rubio, “Polaritonic chemistry: Collective strong coupling implies strong local modification of chemical properties,” *J. Phys. Chem. Lett.* **12**, 508–516 (2020).
- ³²T. Szidarovszky, G. J. Halász, and Á. Vibók, “Three-player polaritons: nonadiabatic fingerprints in an entangled atom-molecule-photon system,” *New J. Phys.* **22**, 053001 (2020).
- ³³M. A. D. Taylor, A. Mandal, W. Zhou, and P. Huo, “Resolution of gauge ambiguities in molecular cavity quantum electrodynamics,” *Phys. Rev. Lett.* **125**, 123602 (2020).
- ³⁴L. S. Cederbaum, “Polaritonic states of matter in a rotating cavity,” *J. Phys. Chem. Lett.* **12**, 6056–6061 (2021).
- ³⁵L. S. Cederbaum and A. I. Kuleff, “Impact of cavity on interatomic Coulombic decay,” *Nat. Commun.* **12**, 4083 (2021).
- ³⁶C. Fábri, G. J. Halász, L. S. Cederbaum, and Á. Vibók, “Born-Oppenheimer approximation in optical cavities: From success to breakdown,” *Chem. Sci.* **12**, 1251–1258 (2021).
- ³⁷C. Fábri, G. J. Halász, L. S. Cederbaum, and Á. Vibók, “Signatures of light-induced nonadiabaticity in the field-dressed vibronic spectrum of formaldehyde,” *J. Chem. Phys.* **154**, 124308 (2021).

- ³⁸E. W. Fischer and P. Saalfrank, “Ground state properties and infrared spectra of anharmonic vibrational polaritons of small molecules in cavities,” *J. Chem. Phys.* **154**, 104311 (2021).
- ³⁹F. J. Garcia-Vidal, C. Ciuti, and T. W. Ebbesen, “Manipulating matter by strong coupling to vacuum fields,” *Science* **373**, eabd0336 (2021).
- ⁴⁰T. E. Li, A. Nitzan, and J. E. Subotnik, “Collective vibrational strong coupling effects on molecular vibrational relaxation and energy transfer: Numerical insights via cavity molecular dynamics simulations,” *Angew. Chem. Int. Ed.* **60**, 15533–15540 (2021).
- ⁴¹B. Cui and A. Nitzan, “Collective response in light-matter interactions: The interplay between strong coupling and local dynamics,” *J. Chem. Phys.* **157**, 114108 (2022).
- ⁴²J. Fregoni, F. J. Garcia-Vidal, and J. Feist, “Theoretical challenges in polaritonic chemistry,” *ACS Photonics* **9**, 1096–1107 (2022).
- ⁴³T. E. Li, B. Cui, J. E. Subotnik, and A. Nitzan, “Molecular polaritonics: Chemical dynamics under strong light-matter coupling,” *Annu. Rev. Phys. Chem.* **73**, 43–71 (2022).
- ⁴⁴M. Reitz, C. Sommer, and C. Genes, “Cooperative quantum phenomena in light-matter platforms,” *PRX Quantum* **3**, 010201 (2022).
- ⁴⁵D. Wellnitz, G. Pupillo, and J. Schachenmayer, “Disorder enhanced vibrational entanglement and dynamics in polaritonic chemistry,” *Commun. Phys.* **5**, 120 (2022).
- ⁴⁶C. Fábri, “Practical guide to the statistical mechanics of molecular polaritons,” *Mol. Phys.* **0**, e2272691 (2023).
- ⁴⁷L.-B. Fan, C.-C. Shu, D. Dong, J. He, N. E. Henriksen, and F. Nori, “Quantum coherent control of a single molecular-polariton rotation,” *Phys. Rev. Lett.* **130**, 043604 (2023).
- ⁴⁸J. Fregoni and S. Corni, “Chapter 7 - Polaritonic chemistry,” in *Theoretical and Computational Photochemistry*, edited by C. García-Iriepa and M. Marazzi (Elsevier, 2023) pp. 191–211.
- ⁴⁹A. Mandal, M. A. Taylor, B. M. Weight, E. R. Koessler, X. Li, and P. Huo, “Theoretical advances in polariton chemistry and molecular cavity quantum electrodynamics,” *Chem. Rev.* **123**, 9786–9879 (2023).
- ⁵⁰J. B. Pérez-Sánchez, A. Koner, N. P. Stern, and J. Yuen-Zhou, “Simulating molecular polaritons in the collective regime using few-molecule models,” *Proc. Natl. Acad. Sci. U.S.A.* **120**, e2219223120 (2023).

- ⁵¹T. Schnappinger and M. Kowalewski, “Nonadiabatic wave packet dynamics with ab initio cavity-Born-Oppenheimer potential energy surfaces,” *J. Chem. Theory Comput.* **19**, 460–471 (2023).
- ⁵²T. Schnappinger, D. Sidler, M. Ruggenthaler, A. Rubio, and M. Kowalewski, “Cavity Born–Oppenheimer Hartree–Fock ansatz: Light–matter properties of strongly coupled molecular ensembles,” *J. Phys. Chem. Lett.* **14**, 8024–8033 (2023).
- ⁵³J. Galego, F. J. Garcia-Vidal, and J. Feist, “Suppressing photochemical reactions with quantized light fields,” *Nat. Commun.* **7**, 13841 (2016).
- ⁵⁴J. A. Campos-Gonzalez-Angulo, R. F. Ribeiro, and J. Yuen-Zhou, “Resonant catalysis of thermally activated chemical reactions with vibrational polaritons,” *Nat. Commun.* **10**, 1–8 (2019).
- ⁵⁵S. Felicetti, J. Fregoni, T. Schnappinger, S. Reiter, R. De Vivie-Riedle, and J. Feist, “Photoprotecting uracil by coupling with lossy nanocavities,” *J. Phys. Chem. Lett.* **11**, 8810–8818 (2020).
- ⁵⁶E. Davidsson and M. Kowalewski, “Simulating photodissociation reactions in bad cavities with the Lindblad equation,” *J. Chem. Phys.* **153**, 234304 (2020).
- ⁵⁷J. Fregoni, G. Granucci, E. Coccia, M. Persico, and S. Corni, “Manipulating azobenzene photoisomerization through strong light-molecule coupling,” *Nat. Commun.* **9**, 4688 (2018).
- ⁵⁸J. Fregoni, G. Granucci, M. Persico, and S. Corni, “Strong coupling with light enhances the photoisomerization quantum yield of azobenzene,” *Chem* **6**, 250–265 (2020).
- ⁵⁹C. Schäfer, M. Ruggenthaler, H. Appel, and A. Rubio, “Modification of excitation and charge transfer in cavity quantum-electrodynamical chemistry,” *Proc. Natl. Acad. Sci. U.S.A.* **116**, 4883–4892 (2019).
- ⁶⁰A. Semenov and A. Nitzan, “Electron transfer in confined electromagnetic fields,” *J. Chem. Phys.* **150**, 174122 (2019).
- ⁶¹A. Mandal, T. D. Krauss, and P. Huo, “Polariton-mediated electron transfer via cavity quantum electrodynamics,” *J. Phys. Chem. B* **124**, 6321–6340 (2020).
- ⁶²D. Wellnitz, G. Pupillo, and J. Schachenmayer, “A quantum optics approach to photoinduced electron transfer in cavities,” *J. Chem. Phys.* **154**, 054104 (2021).
- ⁶³J. B. Pérez-Sánchez and J. Yuen-Zhou, “Polariton assisted down-conversion of photons via nonadiabatic molecular dynamics: a molecular dynamical Casimir effect,” *J. Phys. Chem. Lett.* **11**, 152–159 (2019).

- ⁶⁴I. S. Ulusoy, J. A. Gomez, and O. Vendrell, “Modifying the nonradiative decay dynamics through conical intersections via collective coupling to a cavity mode,” *J. Phys. Chem. A* **123**, 8832–8844 (2019).
- ⁶⁵B. Gu and S. Mukamel, “Manipulating nonadiabatic conical intersection dynamics by optical cavities,” *Chem. Sci.* **11**, 1290–1298 (2020).
- ⁶⁶B. Gu and S. Mukamel, “Cooperative conical intersection dynamics of two pyrazine molecules in an optical cavity,” *J. Phys. Chem. Lett.* **11**, 5555–5562 (2020).
- ⁶⁷M. H. Farag, A. Mandal, and P. Huo, “Polariton induced conical intersection and Berry phase,” *Phys. Chem. Chem. Phys.* **23**, 16868–16879 (2021).
- ⁶⁸T. Szidarovszky, P. Badankó, G. Halász, and Á. Vibók, “Nonadiabatic phenomena in molecular vibrational polaritons,” *J. Chem. Phys.* **154**, 064305 (2021).
- ⁶⁹A. Csehi, O. Vendrell, G. J. Halász, and Á. Vibók, “Competition between collective and individual conical intersection dynamics in an optical cavity,” *New J. Phys.* **24**, 073022 (2022).
- ⁷⁰C. Fábri, G. J. Halász, L. S. Cederbaum, and Á. Vibók, “Radiative emission of polaritons controlled by light-induced geometric phase,” *Chem. Commun.* **58**, 12612–12615 (2022).
- ⁷¹C. Fábri, G. J. Halász, and Á. Vibók, “Probing light-induced conical intersections by monitoring multidimensional polaritonic surfaces,” *J. Phys. Chem. Lett.* **13**, 1172–1179 (2022).
- ⁷²E. W. Fischer and P. Saalfrank, “Cavity-induced non-adiabatic dynamics and spectroscopy of molecular rovibrational polaritons studied by multi-mode quantum models,” *J. Chem. Phys.* **157**, 034305 (2022).
- ⁷³D. Manzano, “A short introduction to the Lindblad master equation,” *AIP Adv.* **10**, 025106 (2020).
- ⁷⁴J. Torres-Sánchez and J. Feist, “Molecular photodissociation enabled by ultrafast plasmon decay,” *J. Chem. Phys.* **154**, 014303 (2021).
- ⁷⁵I. S. Ulusoy and O. Vendrell, “Dynamics and spectroscopy of molecular ensembles in a lossy microcavity,” *J. Chem. Phys.* **153**, 044108 (2020).
- ⁷⁶P. Antoniou, F. Suchanek, J. F. Varner, and J. J. Foley IV, “Role of cavity losses on nonadiabatic couplings and dynamics in polaritonic chemistry,” *J. Phys. Chem. Lett.* **11**, 9063–9069 (2020).

- ⁷⁷G. J. Halász, Á. Vibók, and L. S. Cederbaum, “Direct signature of light-induced conical intersections in diatomics,” *J. Phys. Chem. Lett.* **6**, 348–354 (2015).
- ⁷⁸G. J. Halász, Á. Vibók, N. Moiseyev, and L. S. Cederbaum, “Nuclear-wave-packet quantum interference in the intense laser dissociation of the D_2^+ molecule,” *Phys. Rev. A* **88**, 043413 (2013).
- ⁷⁹C. L. Cortes, M. Otten, and S. K. Gray, “Non-Hermitian approach for quantum plasmonics,” *J. Chem. Phys.* **152**, 084105 (2020).
- ⁸⁰J. McTague and J. J. Foley IV, “Non-Hermitian cavity quantum electrodynamics–configuration interaction singles approach for polaritonic structure with ab initio molecular Hamiltonians,” *J. Chem. Phys.* **156**, 154103 (2022).
- ⁸¹K. Mølmer, Y. Castin, and J. Dalibard, “Monte Carlo wave-function method in quantum optics,” *J. Opt. Soc. Am. B* **10**, 524–538 (1993).
- ⁸²S. Mandal, F. Gatti, O. Bindech, R. Marquardt, and J.-C. Tremblay, “Multidimensional stochastic dissipative quantum dynamics using a Lindblad operator,” *J. Chem. Phys.* **156**, 094109 (2022).
- ⁸³S. Mandal, F. Gatti, O. Bindech, R. Marquardt, and J. C. Tremblay, “Stochastic multi-configuration time-dependent Hartree for dissipative quantum dynamics with strong intramolecular coupling,” *J. Chem. Phys.* **157**, 144105 (2022).
- ⁸⁴C. Cohen-Tannoudji, J. Dupont-Roc, and G. Grynberg, *Atom-Photon Interactions: Basic Processes and Applications* (Weinheim (Wiley-VCH Verlag GmbH and Co. KGaA), 2004).
- ⁸⁵V. Rokaj, D. M. Welakuh, M. Ruggenthaler, and A. Rubio, “Light–matter interaction in the long-wavelength limit: no ground-state without dipole self-energy,” *J. Phys. B: At. Mol. Opt. Phys.* **51**, 034005 (2018).
- ⁸⁶C. Schäfer, M. Ruggenthaler, V. Rokaj, and A. Rubio, “Relevance of the quadratic diamagnetic and self-polarization terms in cavity quantum electrodynamics,” *ACS Photonics* **7**, 975–990 (2020).
- ⁸⁷J. Triana and J. Sanz-Vicario, “Polar diatomic molecules in optical cavities: Photon scaling, rotational effects, and comparison with classical fields,” *J. Chem. Phys.* **154**, 094120 (2021).
- ⁸⁸D. Sidler, T. Schnappinger, A. Obzhairov, M. Ruggenthaler, M. Kowalewski, and A. Rubio, “Unraveling a cavity induced molecular polarization mechanism from collective vibrational strong coupling,” (2023), arXiv:2306.06004 [quant-ph].

- ⁸⁹J. Galego, C. Climent, F. J. Garcia-Vidal, and J. Feist, “Cavity Casimir-Polder forces and their effects in ground-state chemical reactivity,” *Phys. Rev. X* **9**, 021057 (2019).
- ⁹⁰J. Feist, A. I. Fernández-Domínguez, and F. J. García-Vidal, “Macroscopic QED for quantum nanophotonics: Emitter-centered modes as a minimal basis for multiemitter problems,” *Nanophotonics* **10**, 477–489 (2021).
- ⁹¹P. M. Visser and G. Nienhuis, “Solution of quantum master equations in terms of a non-Hermitian Hamiltonian,” *Phys. Rev. A* **52**, 4727–4736 (1995).
- ⁹²C. Fábri, B. Lasorne, G. J. Halász, L. S. Cederbaum, and Á. Vibók, “Striking generic impact of light-induced non-adiabaticity in polyatomic molecules,” *J. Phys. Chem. Lett.* **11**, 5324–5329 (2020).
- ⁹³D. O. Harris, G. G. Engerholm, and W. D. Gwinn, “Calculation of matrix elements for one-dimensional quantum-mechanical problems and the application to anharmonic oscillators,” *J. Chem. Phys.* **43**, 1515–1517 (1965).
- ⁹⁴J. C. Light and T. Carrington Jr., “Discrete-variable representations and their utilization,” *Adv. Chem. Phys.* **114**, 263–310 (2000).
- ⁹⁵R. Meyer, “Trigonometric interpolation method for one-dimensional quantum-mechanical problems,” *J. Chem. Phys.* **52**, 2053–2059 (1970).
- ⁹⁶E. Süli and D. Mayers, *An Introduction to Numerical Analysis* (Cambridge University Press, 2003).